https://doi.org/10.5194/acp-2019-1216
Preprint. Discussion started: 10 February 2020

Atmospheric Chemistry and Physics Discussions

Tropospheric ozone in CMIP6 Simulations

Paul T. Griffiths[1,2], Lee T. Murray[3], Guang Zeng[4], Alexander T. Archibald[1,2], Louisa K. Emmons[5], Ian Galbally[6,7], Birgit Hassler[8], Larry W. Horowitz[9], James Keeble[1,2], Jane Liu[10], Omid Moeini[11], Vaishali Naik[9], Fiona M. O'Connor[12], Youngsub Matthew Shin[1], David Tarasick[11], Simone Tilmes[5], Steven T. Turnock[12], Oliver Wild[13], Paul J. Young[13,14], and Prodromos Zanis[15]

[1]Centre for Atmospheric Science, Cambridge University, UK
[2]National Centre for Atmospheric Science, Cambridge University, UK
[3]Department of Earth and Environmental Sciences, University of Rochester, Rochester, NY USA
[4]National Institute of Water and Atmospheric Research, Wellington, New Zealand
[5]National Centre for Atmospheric Research, Boulder, Colorado
[6]Climate Science Centre, CSIRO Aspendale Victoria Australia
[7]Centre for Atmospheric Chemistry, University of Wollongong, Wollongong, NSW, Australia
[8]Deutsches Zentrum für Luft- und Raumfahrt (DLR), Institut für Physik der Atmosphäre, Oberpfaffenhofen, Germany
[9]NOAA Geophysical Fluid Dynamics Laboratory, Princeton, NJ, USA
[10]Department of Geography, University of Toronto, Canada
[11]Air Quality Research Division, Environment and Climate Change Canada
[12]Met Office Hadley Centre, Exeter, UK
[13]Lancaster Environment Centre, Lancaster University, Lancaster, UK
[14]Centre of Excellence for Environmental Data Science (CEEDS), Lancaster University, Lancaster, UK
[15]Department of Meteorology and Climatology, Aristotle University of Thessaloniki, Greece

Correspondence: Paul Griffiths (paul.griffiths@ncas.ac.uk)

Abstract. The evolution of tropospheric ozone from 1850 to 2100 has been studied using data from Phase 6 of the Coupled Model Intercomparison Project (CMIP6). We evaluate long-term changes using coupled atmosphere-ocean chemistry-climate models, focusing on the CMIP historical and ScenarioMIP ssp370 experiments, for which detailed tropospheric ozone diagnostics were archived. The model ensemble has been evaluated against a suite of surface, sonde, and satellite observations of the past several decades, and found to reproduce well the salient spatial, seasonal and decadal variability and trends. The tropospheric ozone burden increases from 244 ± 30 Tg in 1850 to a mean value of 348 ± 15 Tg for the period 2005-2014, an increase of 40 %. Modelled present-day values agree well with previous determinations (ACCENT: 336 ± 27 Tg; ACCMIP: 337 ± 23 Tg and TOAR: 340 ± 34 Tg). In the ssp370 experiments, the ozone burden reaches a maximum of 402 ± 36 Tg in 2090, before declining slightly to 396 ± 32 Tg by 2100. The ozone budget has been examined over the same period using lumped ozone production (P_{O3}) and loss (L_{O3}) diagnostics. There are large differences (30%) between models in the preindustrial period, with the difference narrowing to 15% in the present day. Both ozone production and chemical loss terms increase steadily over the period 1850 to 2100, with net chemical production (P_{O3}-L_{O3}) reaching a maximum around the year 2000. The residual term, which contains contributions from stratosphere-troposphere transport reaches a minimum around the same time, while dry deposition increases steadily across the experiment. Differences between the model residual terms are explained in terms of variation in tropopause height and stratospheric ozone burden.

https://doi.org/10.5194/acp-2019-1216
Preprint. Discussion started: 10 February 2020

Atmospheric Chemistry and Physics Discussions

1 Introduction

Tropospheric ozone (O_3) is an important component of air pollution and an oxidising species with adverse effects on human health (Jerrett et al., 2009; Turner et al., 2015; Malley et al., 2017) and vegetation (Fowler et al., 2009). It is also a greenhouse gas (GHG) with a radiative forcing of 0.4 Wm^{-2} (Stevenson et al., 2013; Myhre et al., 2013) and plays an important role in controlling the strength of the terrestrial carbon sink (Sitch et al., 2007). Ozone is not emitted directly into the troposphere but is produced there by the photochemical oxidation of carbon monoxide (CO), methane (CH_4) and non-methane volatile organic compounds (NMVOCs) in the presence of nitric oxide (NO) and nitrogen dioxide (NO_2). The tropospheric ozone burden is controlled by the balance between chemical production and loss processes, deposition at the surface and downward transport from the stratosphere.

In addition to its roles as a GHG and air pollutant, ozone is an oxidant and a precursor for the hydroxyl (OH) radical. OH (and by implication ozone) controls the lifetime of methane (Voulgarakis et al., 2013), the second most important anthropogenic GHG after carbon dioxide (Myhre et al., 2013). Oxidant levels mediate formation of secondary aerosols such as sulfate and nitrate and play a major role in the aerosol budget and burden with important consequences for radiative forcing (Shindell et al., 2009; Karset et al., 2018)). Accurate knowledge of ozone and how ozone has evolved since pre-industrial times is therefore critical to our understanding of the radiative forcing from aerosol and GHGs.

The lifetime of ozone in the troposphere varies considerably with location and season, ranging from a few hours in polluted urban regions up to a few weeks in the upper troposphere (Monks et al., 2015) and the global mean tropospheric lifetime is 23.4±2.2 days (Young et al., 2013). Ozone therefore has a sufficiently long lifetime in the troposphere to be affected by climate variability and by the associated changes in large-scale atmospheric circulation patterns that occur on interannual to decadal time scales.

Due to the difficulties of measuring tropospheric ozone on a global scale, the global burden and budget are estimated using global atmospheric chemistry models which include chemistry climate models (CCMs), chemistry transport models (CTMs) and chemistry general circulation models (chemistry GCMs). While the tropospheric ozone burden and distribution during pre-industrial times is unknown from observations (Tarasick et al., 2019), the present-day ozone monitoring network can be used to calculate tropospheric ozone burden and evaluate global atmospheric chemistry models. Multiple satellite products corroborated by the global ozonesonde network indicate a present-day (2010-2014) tropospheric ozone burden of 338±6 Tg in broad agreement with the current range of model estimates (Gaudel et al., 2018).

Recently, Young et al. (2018) presented an updated regional evaluation of tropospheric ozone simulated by models contributing to the Atmospheric Chemistry and Climate Model Intercomparison Project (ACCMIP) using data from: ozonesonde measurements, a new compilation of long-term measurements conducted aboard commercial aircraft of internationally operating airlines (MOZAIC-IAGOS), and a comprehensive database of global surface ozone measurements that was compiled within the Tropospheric Ozone Assessment Report (TOAR) framework. This evaluation revealed that the models are biased

https://doi.org/10.5194/acp-2019-1216
Preprint. Discussion started: 10 February 2020

Atmospheric Chemistry and Physics Discussions

high in the Northern Hemisphere (NH) and low in the Southern Hemisphere (SH), with the biases generally persisting throughout the depth of the troposphere in agreement with previous global model evaluation studies (Fiore et al., 2012; Stevenson et al., 2013). Most CCMs capture the seasonal cycle of surface and free tropospheric ozone over most regions reasonably well, giving confidence in the relative contribution of the seasonal cycle of emissions and meteorology to the simulated seasonal cycle in ozone. However, there are still model deficiencies in simulating the seasonality of free tropospheric ozone in regions such as Equatorial America, Japan and northern high latitudes (Young et al., 2018) and of near-surface ozone over northern and north-eastern Europe (Katragkou et al., 2015), reflecting poor simulation of local and regional dynamics or missing chemical processes. The spatial patterns in annual mean surface ozone and regional features of free tropospheric ozone are generally captured by current global chemistry models (Tilmes et al., 2016; Hu et al., 2017) including the ozone maximum west of southern Africa over the South Atlantic Ocean (Sauvage et al., 2007), the mid-Pacific minimum (Ziemke et al., 2010), and the summertime free tropospheric ozone maximum over the Eastern Mediterranean (Akritidis et al., 2016; Zanis et al., 2014).

The main chemical reactions contributing to tropospheric ozone production are reactions between NO and hydroperoxyl (HO_2) and other peroxyl radicals that are intermediate products of VOC degradation. Ozone chemical production occurs throughout the troposphere, particularly near the surface close to emissions, and also in the upper troposphere via lightning-produced NO_x. Deposition of ozone occurs at the surface via reactive chemical loss to surfaces. In the free troposphere, ozone loss by photolysis to produce O^1D), and the subsequent reaction of O^1D with H_2O, and by chemical destruction involving HO_x are important (Ayers et al., 1992).

The ozone source and sink terms vary between models due to differing approaches in representing the processes involved, and also due to differences in how these budget terms are defined (Stevenson et al., 2006; Young et al., 2013, 2018). Key issues include the representation of NMVOC chemistry which affects chemical production and loss terms, surface loss processes, and stratospheric influences. The definition of the tropopause will also influence the diagnosed burden and any influx from the stratosphere. The Tropospheric Ozone Assessment Report (TOAR) reviewed the ozone budget terms using results from models that took part in ACCENT and ACCMIP model intercomparisons and from recent single model studies (Young et al., 2018). They reported budget terms for the nominal year 2000, calculating a multi-ensemble mean global tropospheric ozone burden of 340 $\pm$ 34 Tg, chemical production of 4937 $\pm$ 656 Tg O_3 per year, chemical loss of 4442 $\pm$ 570 Tg per year, and deposition loss of 996 $\pm$ 203 Tg per year, leaving a residual term of 535 $\pm$ 161 Tg /year, which is assumed to represent the net stratospheric influx.

During the 21st century, changes in climate, stratospheric ozone-depleting substances (ODSs) and emissions of ozone precursor species are expected to be the major factors governing the amount of ozone and its distribution in the stratosphere, the free troposphere and at the surface (Fiore et al., 2015; Revell et al., 2015). Changes in ozone precursor emissions have the largest effect on future tropospheric ozone concentrations, and precursor emission scenarios described by shared socioeconomic pathways (SSPs) and representative concentration pathways (RCPs) show reductions that drive ozone decreases. A strong sensitivity to emission scenarios is supported by previous and recent model results that reveal a net decrease in the global tropospheric burden of ozone in 2100 compared to that in 2000 for all RCPs except RCP8.5, which shows an increase

https://doi.org/10.5194/acp-2019-1216
Preprint. Discussion started: 10 February 2020

Atmospheric Chemistry and Physics Discussions

due to much larger methane concentrations than the other pathways (Stevenson et al., 2006; Naik et al., 2013; Banerjee et al., 2016; Sekiya and Sudo, 2014; Meul et al., 2018; Revell et al., 2015; Young et al., 2013).

The future evolution of methane concentrations is a major source of uncertainty among the scenarios but there are also other sources of uncertainty related to GHG-induced climate change. Future changes in the net influx of ozone from the stratosphere to the troposphere are linked to changes in the stratospheric Brewer-Dobson circulation (BDC) and the amount of ozone in the lowermost stratosphere which are strongly influenced in a changing climate by changes in ODSs and long-lived GHGs. Future decreases in ODSs will lead to an ozone increase throughout the atmosphere with the largest percentage changes in the upper stratosphere and in the high-latitude lower stratosphere (with a particularly large impact on the SH). However, changes in GHGs will lead to a more complex pattern of ozone changes, with increases in the upper stratosphere (from GHG-induced cooling slowing the rate of gas phase ozone loss) and an increase of net stratospheric influx due to a possible strengthening of the BDC, with ODS decreases counteracting such a strengthening of the BDC due to GHG increases (Morgenstern et al., 2018; Polvani et al., 2018, 2019). For the coming decades, future net changes in the BDC depend on the climate change scenario and compliance with the Montreal Protocol. The BDC acceleration in response to increased GHG forcing is a robust finding across a range of atmospheric models with varying representations of the stratosphere (Butchart, 2014; Oberländer-Hayn et al., 2016) although there are still uncertainties in the magnitude (Morgenstern et al., 2018) and attribution of the strengthening. The substantial weakening effect of ODS decreases on the BDC has only recently been established (Morgenstern et al., 2018; Polvani et al., 2018, 2019). Banerjee et al. (2016) reported that a strengthened BDC under the RCP8.5 scenario has the strongest effect on tropospheric ozone in the tropics and subtropics, while stratospheric ozone recovery from declining long-lived ODSs has a larger role in the mid-latitudes and extratropics. Meul et al. (2018) suggested that the global annual mean influx of stratospheric ozone into the troposphere will increase by 53 % between the years 2000 and 2100 under the RCP8.5 greenhouse gas scenario and that this will be smaller for the moderate RCP6.0 scenario, but the relative change in the contribution of ozone of stratospheric origin in the troposphere is of comparable magnitude in both scenarios.

While all studies agree that STE changes will tend to increase future tropospheric ozone, the relative importance of STE versus tropospheric chemistry for future tropospheric ozone trends remains uncertain. A study using new simulations from multiple CCMs finds considerable disagreement among models regarding past and future responses to drivers of tropospheric ozone even when the same scenario is considered, with much of the model spread likely due to the uncertainty in impacts on ozone in the tropopause region driving inter-model variations in STE trends (Morgenstern et al., 2018). In addition to these stratospheric influences, further uncertainty arises from inter-model differences in tropospheric chemistry and physics (such as photolysis, convection, the boundary-layer scheme).

In this study, we examine the evolution of tropospheric ozone and describe the changes to the budget using the common model diagnostics of ozone production, loss and dry deposition to the surface. Our study focuses on transient simulations that were performed for CMIP6. The simulations run from preindustrial times to the present-day (i.e., "historical" simulations of the CMIP6) and from the present-day to end of the 21st century (i.e. "ssp370" of the future ScenarioMIP simulations) (Eyring et al., 2016). Four models including interactive stratospheric chemistry are selected for this analysis, which differs from previous multi-model studies (e.g., Stevenson et al., 2006; Young et al., 2013). CMIP6 builds on the approach of the

https://doi.org/10.5194/acp-2019-1216
Preprint. Discussion started: 10 February 2020

Atmospheric Chemistry and Physics Discussions

CCMI project using long transient simulations but adds more diagnostics and a new, more complete set of emission data, and the most up-to-date, complete/complex set of interactive models. It draws on an improved set of observational constraints via TOAR to provide a comprehensive set of evaluation of the models' performance against well-established metrics (section 3) for recent decades, and evolution of the tropospheric ozone burden and budget over the full period of the experiments of 1850 to 2100 (section 4).

2 Models, Simulations and Configuration Details

2.0.1 GFDL-ESM4

The atmospheric component of the GFDL-ESM4 (Dunne et al., 2019) called AM4.1, includes an interactive tropospheric and stratospheric gas-phase and aerosol chemistry scheme (Horowitz et al., 2019). The model includes 56 prognostic (transported) tracers and 36 diagnostic (non-transported) chemical tracers, with 43 photolysis reactions, 190 gas-phase kinetic reactions, and 15 heterogeneous reactions. The tropospheric chemistry includes reactions for the NO_x-HO_x-Ox-CO-CH_4 system and oxidation schemes for other NMVOCs. The stratospheric chemistry accounts for the major ozone loss cycles (Ox, HO_x, NO_x, ClO_x, and BrO_x) and heterogeneous reactions on liquid and solid stratospheric aerosols as in Austin et al. (2012). The chemical system is solved using an implicit Euler backward method with Newton-Raphson iteration. Photolysis rates are calculated interactively using the FAST-JX version 7.1 code, accounting for the radiative effects of simulated aerosols and clouds. Emissions of biogenic volatile organic compounds (BVOCs), including isoprene and monoterpenes, are calculated online in AM4.1 using the Model of Emissions of Gases and Aerosols from Nature (MEGAN; (Guenther et al., 2006)), as a function of simulated air temperature and shortwave radiative fluxes. Details on the chemical mechanism are included in Horowitz et al. (2019). The gas-phase and heterogeneous chemistry configuration is similar to that used by Schnell et al. (2018). Anthropogenic and biomass burning emissions are prescribed from the dataset of Hoesly et al. (2018) and van Marle et al. (2017) developed in support of CMIP6. Natural emissions of ozone precursors not calculated interactively are prescribed in the same way as in Naik et al. (2013).

The bulk aerosol scheme, including 18 transported aerosol tracers, is similar to that in AM4.0 (Zhao et al., 2018), with the following updates: (1) ammonium and nitrate aerosols are treated explicitly, with ISORROPIA (Fountoukis and Nenes, 2007) used to simulate the sulfate–nitrate–ammonia thermodynamic equilibrium; (2) oxidation of sulfur dioxide and dimethyl sulfide to produce sulfate aerosol is driven by the gas-phase oxidant concentrations (OH, H_2O_2, and ozone) and cloud pH simulated by the online chemistry scheme, and (3) the rate of aging of black and organic carbon aerosols from hydrophobic to hydrophilic forms varies with calculated concentrations of hydroxyl radical (OH). Sources of secondary organic aerosols (SOA) include an anthropogenic source from oxidation of the simulated C_4H_{10} hydrocarbon tracer by hydroxyl radical and a biogenic pseudo-emission scaled to BVOC emissions from vegetation.

https://doi.org/10.5194/acp-2019-1216
Preprint. Discussion started: 10 February 2020

Atmospheric Chemistry and Physics Discussions

2.0.2 UKESM1-LL-0

UKESM1-LL-0 (also abbreviated to "UKESM1" here) is the UK's Earth System Model (Sellar et al., 2019). It is based on the Global Coupled 3.1 (GC3.1) configuration of HadGEM3 (Williams et al., 2018), to which various Earth system components have been added e.g. ocean biogeochemistry, terrestrial carbon/nitrogen cycle, and atmospheric chemistry. The atmospheric and land components are described in Walters et al. (2019). The chemistry scheme included in UKESM1 is a combined stratosphere-troposphere chemistry scheme (Archibald et al., 2019) from the UK Chemistry and Aerosol (UKCA) model, combining the stratospheric chemistry scheme of Morgenstern et al. (2009) with the tropospheric chemistry scheme of O'Connor et al. (2014). A paper describing and evaluating this stratosphere-troposphere scheme in UKESM1 is currently in discussion (Archibald et al., 2019). The aerosol scheme is a two-moment scheme from UKCA, called GLOMAP-mode, and is part of the Global Atmosphere 7.0/7.1 configuration of HadGEM3 (Walters et al., 2019). It models sulphate, sea salt, organic carbon and black carbon. Some improvements to the aerosol scheme for GA7.1 were required to address the strong negative aerosol forcing found with GA7.0 and are documented in Sellar et al. (2019). A detailed description and evaluation of GLOMAP-mode in UKESM1 can be found in Mulcahy et al. (2018). Dust is modelled separately in 6 size bins following a variant of the Woodward scheme.

Anthropogenic and biomass burning emissions are prescribed (Hoesly et al., 2018; van Marle et al., 2017) but emissions of isoprene and monoterpenes are interactive, and are based on the interactive biogenic VOC (iBVOC) emission model (Pacifico et al., 2011). Lightning emissions of NO_x (LNO_x) are also interactive using the cloud top height parameterization of Price and Rind (Price and Rind, 1992, 1993). Other natural emissions are prescribed as climatologies and will be discussed fully in Archibald et al. (2019). For volcanic eruptions, internally-consistent stratospheric AODs and SADs are prescribed for both the volcanic forcing and for the UKCA stratospheric heterogeneous chemistry. A full description and evaluation of the GLOMAP-mode aerosol scheme in UKESM1 (Mulcahy et al., 2018).

2.0.3 CESM2-WACCM

CESM2-WACCM uses the Community Earth System Model version 2, (Emmons et al., 2019), and is a fully coupled Earth System Model. The Whole Atmosphere Community Climate Model version 6 (WACCM6) is coupled to the other components in CESM2. The Parallel Ocean Program version 2 (POP2) (Smith and Gent, 2002; Danabasoglu et al., 2012) includes several improvements compared to earlier versions, including ocean biogeochemistry represented by the Marine Biogeochemistry Library (MARBL), which incorporates the Biogeochemical Elemental Cycle (BEC) ocean biogoechemistry-ecosystem model (e.g., Moore et al., 2013). Additional components are the sea-ice model CICE version 5.1.2 (CICE5) (Hunke et al., 2015) and the Community Ice Sheet Model version 2.1 (CISM2.1), (Lipscomb et al., 2019). The Community Land Model version 5 (CLM5) also includes various updates, including interactive crops and irrigation for the land , and the Model for Scale Adaptive River Transport (MOSART).

CESM2-WACCM has a good representation of the tropospheric dynamics and climate, and also simulates internal variability in the stratosphere, including Stratospheric Sudden Warming (SSW) events on the intraseasonal timescales and the explicitly-

https://doi.org/10.5194/acp-2019-1216
Preprint. Discussion started: 10 February 2020

resolved Quasi-Biennial Oscillation (Gettelman et al., 2019). The CESM2-WACCM model includes interactive chemistry and aerosols for the troposphere, stratosphere and lower thermosphere with 228 chemical compounds, including the MAM4 4-mode Modal Aerosol Model (Emmons et al., 2019). In particular, it includes an extensive representation of secondary organic aerosols based on the VBS model framework (Tilmes et al., 2019) following the approach by (Hodzic et al., 2016). The scheme includes both updates to the SOA formation and removal pathways. MAM4 has been further modified to incorporate a new prognostic stratospheric aerosol capability (Mills et al., 2016). The modifications include mode width changes, growth of sulfate aerosol into the coarse mode, and the evolution of stratospheric sulfate aerosols from natural and anthropogenic emissions of source gases, including carbonyl sulfide (OCS) and volcanic sulfur dioxide (SO2). Anthropogenic and biomass burning emissions are prescribed (Hoesly et al., 2018; van Marle et al., 2017). Biogenic emissions including BVOC are produced from the Model of Emissions of Gases and Aerosols from Nature (MEGAN) version 2.1 (Guenther et al., 2012) and and are also used for SOA formation.

The CESM2-WACCM model includes interactive chemistry and aerosols for the troposphere, stratosphere and lower thermosphere . It simulates 228 compounds, including the MAM4 4-mode Modal Aerosol Model. This version of MAM4 is modified to allow for the simulation of stratospheric aerosols from volcanic eruptions (from their SO_2 emissions) and oxidation of OCS (Mills et al., 2016). The representation of secondary organic aerosols follows the Volatility Basis Set approach (Tilmes et al., 2019).

2.0.4 GISS-E2-1-H

GISS-E2-1-H is the NASA Goddard Institute for Space Studies (GISS) chemistry-climate model version E2.1 using the HYbrid Coordinate Ocean Model (HYCOM). The model configurations submitted for CMIP6 are described in detail by Kelley et al. (2019) and Miller et al. (2020). Here, we use the subset of model configurations that ran with online interactive chemistry. The atmospheric component was run with horizontal resolution of 2° latitude by 2.5° longitude with 40 hybrid sigma-pressure vertical layers extended from the surface to 0.1 hPa (∼28 in the troposphere). Online interactive chemistry follows the GISS Physical Understanding of Composition-Climate INteractions and Impacts (G-PUCCINI) mechanism for gas-phase chemistry (Shindell et al., 2001, 2003, 2006, 2013; Kelley et al., 2019) and the One-Moment Aerosol (OMA) model for the condensed phase (Koch et al., 2006). The gas-phase mechanism includes 146 reactions (including 28 photodissociation reactions) acting on 47 species throughout the troposphere and stratosphere including five heterogeneous reactions. The model advects 26 aerosol particle tracers and 34 gas-phase tracers. Anthropogenic and biomass burning emissions are prescribed following the CMIP guidelines. Lightning NO_x emissions are calculated online in deep convection as described by Kelley et al. (2019). Soil microbial NO_x emissions are prescribed from climatology. Biogenic emissions of isoprene are calculated online and respond to temperature (Shindell et al., 2006), but are prescribed for alkenes, paraffins and terpenes. Methane is prescribed as a surface boundary condition but allowed to advect and react with the chemistry. The atmosphere is coupled to the HYCOM ocean model (Sun and Bleck, 2006; Romanou et al., 2013) with an $\sim 1°$ tripolar grid with 32 vertical levels. GISS-E2-1-H did not submit the diagnostics necessary for calculating grid-box volume by time of article submission, and therefore was unable to be included in the assessment of the ozone chemical budget.

https://doi.org/10.5194/acp-2019-1216
Preprint. Discussion started: 10 February 2020

2.1 Simulations

For this review, we used available data from the CMIP Historical experiments from UKESM1 (Tang et al., 2019) , GFDL-ESM4 (Krasting et al., 2018), GISS-E2-1-G (NASA Goddard Institute For Space Studies (NASA/GISS), 2019) and CESM2-WACCM (Danabasoglu, 2019a). For ScenarioMIP ssp370 experiments we used data archived by UKESM1 (Good et al., 2019), GFDL-ESM4 (John et al., 2018) and CESM2-WACCM (Danabasoglu, 2019b). We analysed those models that had archived sufficient data to the Earth System Grid Federation Peer-to-Peer system to permit accurate characterisation of the tropospheric ozone burden. In practice this meant, we used archived ozone data from the AERmon characterisation of the tropospheric ozone burden (o3) on native model grids, along with data on the tropopause pressure using the WMO definition of the tropopause (ptp). For the budget calculations, dryo3, o3prod, o3loss along with airmass, temperature and pressure diagnostics were used from the AERmon realm. This limited us to four models for the ozone evaluation (CESM2-WACCM, GFDL-ESM4, GISS-E2-1-H, UKESM1-0-LL) and three models (CESM2-WACCM, GFDL-ESM4, UKESM1-0-LL) for budget calculations.

2.2 Emissions

Figure 1 shows the emissions used in the CMIP6 models. Data for the period 1850 to 2014 were taken from the CMIP "historical" experiment, and for the period 2015 to 2100 from the ScenarioMIP "ssp370" experiment.

CO emissions were calculated using the output emico variable output by each model. Anthropogenic NO_x emissions used in each model were calculated as follows: for UKESM1-0-LL, the eminox variable was used which is the sum of anthropogenic, open-burning, soil, and aircraft NO_x emissions; for GFDL-ESM4, the eminox variable represents anthropogenic, open-burning, soil, aircraft, and lightning NO_x emissions, so the accompanying emilnox (lightning) output for this model was subtracted to calculate anthropogenic NO_x; finally, for CESM2-WACCM, the eminox variable was used which consists of anthropogenic, open-burning, and soil NO_x emissions, so a small fraction of anthropogenic NO_x emissions are missing. Biogenic emissions were calculated using the emibvoc variable.

The CO and NO_x tropospheric burdens were calculated by applying a tropospheric mask derived from each model's tropopause pressure/height output. The NO_x burden was determined as the sum of the NO and NO_2 mole fraction outputs.

The prescribed methane lower boundary concentrations are described in Meinshausen et al. (2019). Over the ssp370 period, global methane concentrations increase monotonically.

3 Evaluation of tropospheric ozone over recent decades

Figure 2 shows the present-day spatial distribution of ozone and its inter-model variability in the CMIP6 ensemble. The spatial patterns are broadly consistent with observations (see Sects. 3.1-3.4) and those of earlier model intercomparison studies (e.g., Stevenson et al., 2006; Young et al., 2013). Zonal mean mixing ratios are highest in the upper troposphere, especially in the extratropics, reflecting longer chemical lifetimes at altitude (Fig. 2a). Ozone is also higher in the NH relative to the SH, reflecting higher rates of stratospheric downwelling (e.g., Rosenlof, 1995) and surface ozone precursor emissions. The model ensemble

https://doi.org/10.5194/acp-2019-1216
Preprint. Discussion started: 10 February 2020

members are in relative good agreement, with a standard deviation of less than 25 % throughout most of the troposphere. The greatest absolute and relative differences in mixing ratio occur in the upper troposphere. This reflects relatively large inter-model variability in the simulated mean tropopause pressure (± 30 hPa). The tropopause acts as a dynamical barrier that separates the high-ozone air of the stratosphere from the low-ozone air of the troposphere. Therefore, simulated differences in tropopause height manifest as large differences in ozone mixing ratio in the upper troposphere and lower stratosphere (UT/LS) region. Furthermore, variations in tropopause pressure allow for more or less air mass to exist in the troposphere (± ∼3 %), also contributing to variations in tropospheric columns of ozone (TCO) between models, especially in the northern extratropics (Fig. 2e-f). Inter-model variability in TCO (Fig. 2e) is about twice as high as earlier model intercomparison studies (e.g., Young et al., 2013) due to our use of the pressure tropopause rather than a chemical tropopause (see Sect. 3.4). In addition, ozone mixing ratios vary relatively largely between models in the tropics, especially in the boundary layer and the UT/LS region. The latter is of interest due to the importance of absorption of outgoing longwave radiation for radiative forcing in this region (e.g., Forster and Shine, 1997).

3.1 Surface ozone

Figure 4 compares the CMIP6 model ensemble to four surface ozone stations with the longest available *in situ* sampling record: Mauna Loa, Hawai'i, USA (MLO, 19.5°N, 155.6°W, 11 m.a.s.l., 1957-present), the South Pole (SPO, 90°S, 59°E, 2840 m.a.s.l., 1961-present), Barrow, Alaska, USA (BRW, 71.3°N, 156.6°W, 11 m.a.s.l., 1973-present), and Cape Grim, Tasmania, Australia (CGO, 40.7°S, 144.7°E, 94 m.a.s.l., 1982-present). These measurements in remote background locations are useful constraints for evaluation of trends in the tropospheric ozone budget. For a more thorough evaluation and examination of surface ozone in the CMIP6 simulations, including implications for surface air quality, we refer the reader to the CMIP6 surface ozone companion paper (Turnock et al., 2020).

Mauna Loa is especially useful for evaluating trends in tropospheric ozone. In addition to a long historical record, it is a remote mountain site that frequently samples free tropospheric air masses. Here we use monthly average surface ozone measured using a Regener type potassium iodide (KI) automatic ozone analyser for 1957-1959 and a UV photometric analyser for 1974-2014, obtained from Owen Cooper (NOAA ESRL, *pers. comm.*, 2019). Barrow data measured using a UV photometric analyser for 1973-2014 was obtained from the TOAR database. In the time before and after polar sunrise there are significant ozone-depletion events in surface air that are large enough to affect annual mean ozone levels (e.g., Oltmans and Levy, 1994; Helmig et al., 2007). South Pole measured using a Regener type potassium iodide (KI) automatic ozone analyser for 1961-1963, a corrected Regener type chemiluminescent automatic ozone analyser for 1964-1966, an Electrochemical Cell analyser for 1967-1973 and a UV photometric analyser for 1975-2014 were also obtained as monthly averages from Owen Cooper (NOAA ESRL, *pers. comm.*, 2019). Cape Grim data measured using a UV photometric analyser for 1982-2014 are available as hourly averages from the WMO World Data Centre for Reactive Gases. Monthly observations were converted to annual averages for those with 9 months or more of data. Corrections to the data to account for the different ozone analysers operated during the historical period have been applied to the MLO and SPO data using the framework described by Tarasick

https://doi.org/10.5194/acp-2019-1216
Preprint. Discussion started: 10 February 2020


Atmospheric Chemistry and Physics Discussions

et al. (2019). We sample the models at the surface level for Barrow, Cape Grim and the South Pole, and at the 680 hPa level for Mauna Loa.

The models overestimate surface ozone concentrations at the two NH sites by 3-4 ppbv, and underestimate surface ozone at the two SH sites by 2-7 ppbv. In particular, the models significantly underestimate surface ozone at the South Pole. These discrepancies may reflect biases associated with comparing point data to a much coarser model grid cell.

At Barrow, Mauna Loa and Cape Grim, observed surface ozone has increased on average by 0.5-2.0 ppbv per decade (2-4 % per decade) since measurements began. Despite the mean bias, the models well-capture the magnitude of the decadal trends in response to climate and emission forcings. Over Antarctica, observations show an initial decrease from the 1960s through the mid-1990s, before ozone began rising, resulting in no significant trend during this period. The models underestimate the magnitude of the observed reduction, and consequently, simulate a small growth here.

3.2 Vertical, meridional and seasonal ozone distribution

Figure 3 compares the vertical, meridional and seasonal distribution of ozone in the CMIP6 ensemble to climatological measurements from ozonesondes (balloons). We use sonde measurements archived by the World Ozone and Ultraviolet Radiation Data Centre (WOUDC) of the World Meteorological Organization/Global Atmosphere Watch Program (WMO/GAW). The data was accessed on Nov. 4, 2019 from https://doi.org/10.14287/10000008. A total of 23,392 profiles using Carbon-Iodine (Komhyr, 1969), ECC (Komhyr, 1971), and Brewer-Mast (Brewer and Milford, 1960) sondes from 82 sites world-wide were aggregated over the period 2005-2014. Sondes show a modest high bias in the troposphere of about 1-5 % $\pm$ 5 % when compared to more accurate UV-absorption measurements (Tarasick et al., 2019). Measurement precision is $\pm$3-5 % and the overall uncertainty in ozone concentration is less than 10 % in the troposphere (Kerr et al., 1994; Smit et al., 2007; Tarasick et al., 2016, 2019).

The models reproduce the increase in ozone with altitude and from south to north, and well reproduce the seasonal cycle of ozone in the tropics and northern extratropics (r^2 all greater than 0.64). Note that the northern hemispheric overestimate and southern hemispheric seen at the surface (Sect. 3.1) extends into the lower free troposphere. The ensemble mean is biased high by about 10 % in the NH, although always falls within the range of interannual variability in the observations (vertical lines). The ensemble reproduces the magnitude and seasonality of the southern tropics better than the other regions, although it fails to reproduce the timing and magnitude of the October peak associated with the zonal wave-one South Atlantic ozone maximum (Fishman et al., 1990, 1991; Shiotani, 1992; Thompson and Hudson, 1999; Thompson et al., 2000; Thompson, 2003b; Sauvage et al., 2006). The model ensemble performs worst in the southern extratropics, resulting from seasonal behavior anti-correlated with the observations in some models. CMIP6 shows nominal improvements in certain regions such as the southern tropics with respect to biases and correlations reported by the earlier ACCMIP (Young et al., 2013) and ACCENT (Stevenson et al., 2006) studies, although it is difficult to evaluate given the smaller number of models in the CMIP6 (4) versus ACCMIP (15) and ACCENT (26) studies, and given different periods of evaluation.

https://doi.org/10.5194/acp-2019-1216
Preprint. Discussion started: 10 February 2020

Atmospheric Chemistry and Physics Discussions

3.3 Tropospheric ozone column abundance

Satellites provide daily near-global coverage of tropospheric columns of ozone (TCO), the amount of ozone integrated from the surface to the tropopause, typically given in Dobson Units (1 DU $\equiv 2.69 \times 10^{20}$ molecules m^{-2}). Figure 5 compares the seasonality of TCO in the model ensemble to that of the Ozone Monitoring Instrument/Microwave Limb Sounder (OMI/MLS) product (Ziemke et al., 2006). The OMI/MLS product is the residual of the OMI total ozone column and the MLS stratospheric ozone column, available as gridded $1° \times 1.25°$ monthly means, and is provided from 60°S to 60°N due to its reliance on solar backscattered UV radiation. Here we use the data for 2005-2014 downloaded in Nov. 2019 from https://acd-ext.gsfc.nasa.gov/Data_services/cloud_slice/new_data.html.

The model ensemble captures the salient features of spatial-seasonal patterns in TCO from OMI/MLS. This includes zonal-wide maxima in the subtropics (where isentropes intersect the tropopause), greater TCO in the NH, minima over the remote Pacific and Antarctic, and the zonal-wave pattern over the South Atlantic ocean. On average, the models overestimate TCO in the NH and Indian Ocean by up to 25 % versus OMI/MLS, and underestimate ozone in the remote Pacific and Southern Ocean, yielding small net positive biases when integrated over the whole region (+2 DU or 7-9 % in all seasons). The models show greatest disagreement in summertime extratropical TCO, especially in the high Arctic, but OMI/MLS is not available here.

Figure 6 evaluates annual mean TCO in the model ensemble versus OMI/MLS and the Trajectory-mapped Ozonesonde dataset for the Stratosphere and Troposphere (TOST). TOST is a global three-dimensional dataset of tropospheric and stratospheric ozone, derived from the ozonesonde record (Liu et al., 2013b, a). TOST determines TCO using 96-hour forward and backward trajectory calculations of the ozone profiles using the Hybrid Single-Particle Lagrangian Integrated Trajectory (HYSPLIT) particle dispersion model (Draxler and Hess, 1997, 1998) driven by the global NOAA National Centers for Environmental Prediction/National Center for Atmospheric Research (NCEP/NCAR) pressure level meteorological reanalysis. By assuming ozone production and loss to be negligible, the ozone is mapped to other locations and times using a 3-dimensional grid of $5° \times 5° \times$ 1 km. TCO is calculated from the surface to the tropopause, which is defined using the WMO 2 K/km lapse-rate definition applied to the NCEP reanalysis. Over mountainous areas a topographic correction is made in order to address an apparent bias in TCO over high mountains. TOST has been evaluated using individual ozonesondes, excluded from the mapping, by backward and forward trajectory comparisons, and by comparisons with aircraft profiles and surface monitoring data (Tarasick et al., 2010; Liu et al., 2013a, b). Differences are typically about 10 % or less, but there are larger biases in the UT/LS, the boundary layer, and in areas where ozonesonde measurements are very sparse. The accuracy of the TOST product depends largely on the accuracy of HYSPLIT and the meteorological data on which it is based.

The TOST data presented here uses the troposphere-only dataset, which explicitly excludes trajectories originating in the stratosphere. This avoids including stratospheric air, with its very high ozone content, when the NCEP tropopause is higher than the climatological tropopause (i.e. the ozone tropopause). If the same calculations are made using the full-profile TOST dataset, the calculated burden is on average 42 Tg (about 15 %) larger.

https://doi.org/10.5194/acp-2019-1216
Preprint. Discussion started: 10 February 2020

Atmospheric Chemistry and Physics Discussions

The models agree with the TOST product in much of the tropics, except in the remote Pacific, where they are biased low, qualitatively consistent with the OMI/MLS product. Since the TOST product is on average lower than OMI/MLS, especially in higher latitudes, the models are biased even higher with respect to the TOST data than OMI/MLS (+6 DU and 23 %). ‘

3.4 Tropospheric ozone burden

Figure 7 compares the present-day tropospheric ozone burden to seven space-based satellite products and the ozonesonde-derived TOST product. The satellite-derived products include the annual mean burdens for 60°S-60°N from OMI/MLS, IASI (Infrared Atmospheric Sounding Interferometer)-FORLI (Fast Optimal Retrievals on Layers), IASI-SOFRID (SOftware for a Fast Retrieval of IASI Data), GOME (Global Ozone Monitoring Experiment)/OMI-SOA (Smithsonian Astrophysical Observatory), OMI-RAL (Rutherford Appleton Laboratory), SCIAMACHY (SCanning Imaging Absorption SpectroMeter for Atmospheric CHartographY), and TES (Tropospheric Emission Spectrometer) reported by Gaudel et al. (2018). The TOST record has been calculated since 1980, but is most accurate beginning in 1998 when sonde measurements began in the tropics as part of the Southern Hemisphere Additional OZonesondes (SHADOZ) campaign (Thompson, 2003a). The satellite burdens span a range of values (∼250-350 Tg) consistent with the multi-model mean (MMM) and standard deviation, reflecting uncertainties in the tropopause definition (Gaudel et al., 2018). TOST is consistently lower than most satellite products and the model ensemble. Despite the spread in mean value, the models and observations largely agree in the magnitude of the increasing trend following 1997 (0.88 ± 0.14 Tg yr^{-1} in the CMIP6 ensemble vs. 0.65 ± 0.14 Tg yr^{-1} in TOST vs. 0.83 ± 0.85 Tg yr^{-1} in the satellite ensemble).

The right two panels of Fig. 7 demonstrate the sensitivity of the tropopause burden to the definition of the tropopause applied. Earlier model intercomparison studies generally utilized a chemical tropopause defined at the 150 ppbv ozone isopleth, since most models did not archive TCO calculated as an online diagnostic or tropopause pressure, and there is no clear tropopause definition for tracers. However, there is a relatively large amount of ozone by mass in the upper troposphere, and the local column and global burden is sensitive to the exact definition applied. Model groups taking part in the CMIP6 experiments were asked to archive both monthly mean tropopause pressure as well as monthly mean TCO as calculated online with the dynamically varying tropopause and ozone concentrations. We calculate the tropospheric ozone burden using the monthly mean tropopause pressure in two different ways: first, excluding the mass of ozone in the layer containing the tropopause (as commonly implemented; “exclusive”; yellow); and second, including the mass of ozone between the bottom of the layer containing the tropopause and the tropopause itself (“inclusive”; orange). The ozone mixing ratio in the layer containing the tropopause reflects a mixture of tropospheric and stratospheric air, and may be biased toward the higher stratospheric values. However, there is a potentially non-negligible amount of tropospheric ozone mass in this level, as reflected in the difference between the inclusive and exclusive calculations of the tropospheric burden in Fig. 7b-c. Either way, the inter-model spread in tropospheric burdens is much higher when calculated with the pressure tropopause than the chemical tropopause (red). This is because there is large inter-model variability in the tropopause pressure (Fig. 2), and because the chemical tropopause by definition somewhat limits the amount of ozone mass in the troposphere. That being said, TCO calculated using the monthly mean chemical tropopause ends up being most similar in mean and variability to the online TCO diagnostic in the two models

https://doi.org/10.5194/acp-2019-1216
Preprint. Discussion started: 10 February 2020

Atmospheric Chemistry and Physics Discussions

that archived it using the dynamically-varying online pressure tropopause and ozone (orange-red). In this study, we elect to use the exclusive pressure tropopause definition for defining the tropopause for purposes of the following budget calculations, but recommend future studies archive and explore the sensitivity of results to multiple definitions of the tropopause, especially with online TCO diagnostics.

4 Evolution of tropospheric ozone burden and budget over the period 1850-2100

4.1 Evolution of tropospheric ozone burden from 1850 to 2100

Figure 8 shows the evolution of the tropospheric ozone burden for the three models together with the multi-model mean. The figure shows a large increase in tropospheric ozone burden, consistent with the increase in emissions of ozone precursors from the pre-industrial (PI) to the present day period (PD). The burden increases by 104 Tg from the PI (MMM 244 $\pm$ 30 Tg) to the PD (348 $\pm$ 15 Tg), with the most rapid change to burden occurring between 1950 and 1990. Figure 8 shows that the burdens calculated in CMIP6 models are consistent with those from ACCMIP time slice experiments for 1850, 1930, 1980 and 2000. There is good agreement between the two data sets, with a similar range in calculated model burden.

Good agreement is seen between the CMIP6 multi-model mean burden and separate estimates from TOAR (derived from observational estimates of the whole-troposphere ozone burden using IASI and TOST data) and with the ACCMIP multi-model mean. The CMIP6 burden for the period 1990-2014 is however significantly higher than the TOST burden data presented above (section 3.4) for the same period. The origin of this discrepancy is not yet clear, and may emerge as more models with varying ozone distributions and tropospheric extent become available. Despite the high model bias with respect to these observational data, it is clear that a similar trend is observed for both model and observations, with both the TOST-derived burden and the CMIP6 historical mean burden increasing by around 15 Tg over the period 2000-2015. Further observational constraint is provided by the study of (Yeung et al., 2019) who used isotope data to estimate that the change in ozone burden was no less than 40 % over the period 1950-2014. In CMIP6, the change in MMM is from 280 Tg to 350 Tg over this period, a change of 20 %, consistent with this constraint.

The evolution in burden from 2014 to 2100 is shown for the ssp370 scenario. The burden increases by a further 40 Tg over the period 2015-2100, reaching a maximum value of 402 Tg in 2090. The major ozone precursors are projected to increase in the early part of ssp370 up to 2030 before beginning to level off after 2050 as in Figure 1. As anthropogenic NO_x and CO emissions in ssp370 are projected to stabilise, the continued increase in ozone burden indicates an increasingly significant role for other ozone precursors, particularly BVOCs, in this scenario, and a possible role for climate-driven effects.

The range in simulated burden varies across the three simulations, with the range narrowing from 60 Tg in PI conditions to 22 Tg for 2005-2015. This may be connected to the wider spread in BVOC emissions in at the start of the historical simulation and at the end of the ssp370 experiment. Over the course of the simulations, the intermodel range in BVOC emissions narrows, before increasing again after 2000, Figure 1, but at different rates and by differing amounts. The behaviour of BVOC emissions is consistent with the range of simulated burdens. For PI conditions, the model with the largest BVOC emissions, UKESM1,

https://doi.org/10.5194/acp-2019-1216
Preprint. Discussion started: 10 February 2020


Atmospheric Chemistry and Physics Discussions

has the largest burden, while CESM2-WACCM, which has the largest BVOC emissions at the end of the ssp370 experiment, has the highest modelled ozone burden in 2100.

4.2 Regional changes

Figures 9-10 show the historical changes in tropospheric ozone distribution in the CMIP6 ensemble since the preindustrial. Over the historic period, ozone increases throughout the troposphere, with greatest increases occurring in the NH. The largest relative changes occur near the surface in the NH, especially downwind of eastern North America and East Asia, where the rise in ozone precursor emissions (Fig. 1) were predominantly located. Of the three periods explored, the bulk of the increase in ozone occurred between the 1930s and 1980s. Since the 1980s, most of the increases were located in South and East Asia, and the southern tropics and subtropics, reflecting the implementation of aggressive precursor emission controls in North America and Europe.

Figures 11-12 show the future changes in tropospheric ozone distribution in the CMIP6 ensemble relative to the present day. Future changes are expected to be less dramatic than the preindustrial rise, reflecting the reduction in in NO_x emissions and relative stabilization of CO emissions in the ssp370 scenario (Fig. 1). Despite the precursor emission reductions, tropospheric ozone still increases across the 21st century, particularly in the subtropical upper troposphere, probably reflecting an increase in stratospheric downwelling associated with a GHG-driven acceleration to the BDC (Garcia and Randel, 2008), as well as an increase in the height of the tropopause. The models predict that TCO decreases over the remote Pacific, likely reflecting precursor emission reductions coupled with an increase in ozone-destroying tropospheric water vapour.

4.3 Ozone budget

Figure 13 shows the evolution of globally integrated ozone dry deposition, net chemical ozone production, and the inferred net stratospheric to tropospheric transport (STE: derived as the "residual" in the ozone budget).

Ozone dry deposition increases over the period 1850 to 2100. The variation in dry deposition largely reflects the evolving ozone burden which increases over the PI to PD period. There are large differences in ozone dry deposition between UKESM1 (633 Tg yr^{-1} in 1850) and the other two models (approx. 460 Tg yr^{-1}) before 1950, but the differences are smaller after the year 2000 (mean 830 $\pm$ 40 Tg yr^{-1}). Figure 14 shows that the higher dry deposition fluxes in UKESM1 are mostly in tropical regions, with significantly higher deposition in the Amazon, SE Asia and sub-Saharan Africa. This greater efficiency is likely due to the interactive ozone deposition scheme in UKESM1, which uses land-use cover and vegetation type to calculate deposition fluxes (Hardacre et al., 2015), and may be also due to the higher BVOC emissions in UKESM1 (Figure 1) which lead to higher ozone production at the surface. Both figures show that, while UKESM1 shows the larger deposition fluxes for all times, the PI-PD change is smallest for this model at 234 Tg, being less than that for the other models of around 330 Tg (Table 1), and reflecting the smaller relative change in ozone burden that drives the deposition process. Note that there are slight decreases of dry deposition in tropical western Africa and the South America (in CESM2-WACCM) presumably due to land use changes from the PI to PD.

https://doi.org/10.5194/acp-2019-1216
Preprint. Discussion started: 10 February 2020

Atmospheric Chemistry and Physics Discussions

Figure 13 shows a more complex behaviour in net chemical production (defined as $P_{O3} - L_{O3}$). For this analysis, P_{O3} is defined as the sum of reaction fluxes through HO_2/RO_2 + NO reactions, and L_{O3} as the sum of $O(^1D)$+H_2O, O_3+HO_2 and OH, and O_3+alkenes. There is a small increase in NCP over the period 1850-1930, at which point there is a more rapid rise in both the burden and the emission of tropospheric ozone precursors, see Figure 1. This rapid increase continues until around 1980 at which the growth in emissions slows. The projected emissions, and NCP, reach a maximum between 2030 and 2050, and subsequently stabilise.

While similar behaviour across time is seen for all models, they show different absolute responses to the increase in emissions and different structural features. The PI to PD change in NCP is 585 Tg yr^{-1} for UKESM1, compared to 460 Tg yr^{-1} for CESM2-WACCM and 400 Tg yr^{-1} for GFDL-ESM4.

Figure 15 shows the variation in vertically integrated zonal mean ozone production over the period 1850 to 2100. In the PI, the main region of ozone production is located in the tropics from emissions of NO_x from biomass burning at the surface and NO_x production in the UT from lightning. In the PI period, NCP is close to zero for CESM2-WACCM and GFDL-ESM4, similar to values reported for 1900 in (Wild and Palmer, 2008). The higher production in UKESM1 can be correlated with the significantly higher BVOC emissions in the PI period, as seen in Figure 1.

In the 20^{th} century, ozone production can be seen to commence in NH mid-latitudes in response to the increase in anthropogenic emissions in these regions. There is a substantial increase in the extent of regions of strong, positive NCP in the NH extratropics from the mid 20^{th} century onwards, and some expansion of the region of positive NCP into the southern subtropics can be seen beginning around 1980. Around the year 2010, NCP reaches a maximum and then begins to decline, presumably in response to the projected decrease in emissions of tropospheric ozone precursors in the later part of the 21^{st} Century (Revell et al., 2015).

Net ozone destruction occurs predominantly in the SH, due to a combination of low emissions and chemical ozone destruction via ozone photolysis and reaction with HO_x radicals in the free troposphere and over the oceans (Cooper et al., 2014). Ozone destruction in this region reaches a minimum around 2000, presumably due to a shift in emissions southward during the later 20^{th} century (Zhang et al., 2016). In the 21^{st} century, there is a pronounced increase in ozone destruction in the SH mid-latitudes, reflecting a warmer and wetter future climate that promotes ozone chemical destruction through the reaction of $O(^1D)$ and H_2O following ozone photolysis (Stevenson et al., 2006) and higher concentrations of HO_x radicals (Doherty et al., 2013; Johnson et al., 1999). In the tropics, there is a strong net ozone destruction in CESM2-WACCM over the whole period, with an increase towards the end of 21^{st} century; this tropical feature is much weaker in the other two models and there is even slightly net positive ozone production in UKESM1 before around 2020.

Figure 16 shows that both chemical production and loss terms, P_{O3} and L_{O3} increase over the 20^{th} century, but that these terms increase at different rates over the period of the integrations. Chemical production increases rapidly over the 20^{th} century, particularly in CESM2-WACCM and UKESM1, and the rate of increase slows in the 21^{st} century as projected emissions reductions begin to have an impact. Chemical destruction also increases over the entire period, largely following ozone burden increases, but also reflecting increases in HO_x radicals, as discussed above, and stratospheric ozone recovery. After 2030, the destruction rate increases faster than production, and NCP begins to decrease.

https://doi.org/10.5194/acp-2019-1216
Preprint. Discussion started: 10 February 2020

Atmospheric Chemistry and Physics Discussions

The ozone burden in UKESM1 is noticeably higher than other models, particularly in the PI. Figure 17 shows the ozone production efficiency (OPE; defined as moles of ozone produced per mole of NO_x emitted) for the three models used here. The OPE is a function of the background NMVOC mixing ratio, and the higher VOC emissions in UKESM1 appear to account for much of the variation in OPE between models in the period 1850-1900. OPE declines across the 20th century, but recovers somewhat in the 21st. Here ozone production responds more sensitively to increasing NO_x, with implications for air quality.

While there is a large inter-model spread in NCP and dry deposition terms (i.e., substantially higher values in UKESM1), there are similar residual terms in the ozone budget (i.e., the inferred net stratospheric influx) before the 1950s. These values decrease sharply after 1970 partly due to the effect of stratospheric ozone depletion. This is a robust feature as models consistently show reduced ozone STE in the present-day compared to pre-industrial times, due to stratospheric ozone depletion, although the magnitude of the estimated change is model-dependent (WMO Ozone Assessment, 2018).

After the year 2000, the residual terms starts to increase in all models coinciding with the expected ozone recovery (decrease in ozone depleting substances) and the increased BDC associated with increasing GHGs. Several recent studies with CCMs including a stratospheric ozone tracer provide evidence that both the acceleration of the BDC and stratospheric ozone recovery will tend to increase the future global tropospheric ozone burden through enhanced STE with the magnitude of the change depending on the RCP scenario (Banerjee et al., 2016; Meul et al., 2018; Akritidis et al., 2019). This projected increase in STE associated with climate change and ozone recovery offsets decreases in net chemical production associated with reductions in ozone precursor emissions, in agreement with Sekiya and Sudo (2014). Note that the very low residual in UKESM1 is likely the result of a much larger stratospheric ozone depletion (shown in 18) in this model leading to reduced net stratospheric influx.

Models differ in their simulations of stratospheric ozone, which inevitably affects tropospheric ozone through stratosphere-troposphere coupling. Figure 18 shows preindustrial zonal mean ozone (PI: averaged over 1850-1859), changes in ozone between the PI and the present-day periods (PD; averaged over 1995-2004), and the change between PD and the end of the 21st century (2090-2100) in all three models. In the PI case, UKESM1 has the largest ozone mixing ratios throughout the troposphere among the three models, which is associated with its large ozone production (Figure 15) and the net ozone production (Figure 16). The larger PI surface ozone mixing ratio in UKESM1, especially in the SH, is also reflected in its enhanced dry deposition (Figure 14). The propagation of ozone from the stratosphere to the troposphere is evident in all three models, and the stratospheric intrusion through the mid-latitudes seems deeper in CESM2-WACCM and GFDL-ESM4; indeed, slightly larger inferred STE (i.e. the residual in Table 1) are shown in these two models. Figure 18 shows the smaller tropospheric ozone burden increase from PI to PD in UKESM1 is likely the result of stratospheric ozone depletion being the most pronounced among the three models. Note that from the PI to PD there are substantial ozone increases in the high-latitude NH lower stratosphere in both CESM2-WACCM and GFDL-ESM4, which would enhance stratosphere-to-troposphere transport of ozone and which would explain the larger ozone burden increase in these two models compared to UKESM1, despite the larger increase of NCP in UKESM1 (from 279 to 830 Tg/yr compared to an increase from 78 to 530 in CESM2-WACCM and from 86 to 466 in GFDL-ESM4; Table 1). All three models show tropopause height increases between PI and PD at southern high latitudes due to circulation changes associated with increasing GHGs and ozone depletion, but with a smaller but visible increase in the NH mid-latitides in UKESM1. From PD on into the future, all three models show pronounced

https://doi.org/10.5194/acp-2019-1216
Preprint. Discussion started: 10 February 2020

Atmospheric Chemistry and Physics Discussions

stratospheric ozone increases, which visibly impact the tropospheric ozone abundance. Again, UEKSM1 shows the smallest increase in tropospheric ozone among the three models, which also shows some decrease of ozone along the tropopause that might be linked to the rise of the tropopause height in future climate. However, such a feature is not obvious in the other two models which also show a slight increase of the tropopause height.

5 Summary and conclusions

We have analysed the evolution of tropospheric ozone in CMIP6 CMIP Historical and ScenarioMIP ssp370 experiments, a "middle of the road" pathway involving regional rivalry. Ozone has been evaluated against a broad range of observations spanning several decades, and we have determined the evolution of the tropospheric ozone burden over the period 1850-2100. For this analysis, we have concentrated on coupled atmosphere-ocean experiments using whole atmosphere chemistry and interactive ozone. We excluded those models that use simplified chemistry which have been shown to yield low ozone burdens, with the availability of data limiting us to an analysis of ozone burden in four models and the ozone budget for three models.

We evaluated these CMIP6 models against a suite of surface, sonde and satellite products for the recent past. The models tend to overestimate ozone in the northern hemisphere and understimate ozone in the southern hemisphere. Nevertheless, the models well-reproduce the spatial and seasonal variability in the tropospheric ozone distribution, and capture the observed increasing trends in tropospheric ozone since at least 1998.

However, a key uncertainty identified by this analysis regards the definition of the troposphere. We compared definitions based on the chemical tropopause (as traditionally applied) versus the pressure tropopause and online tropospheric ozone diagnostics. All three varied significantly from one another, and we recommend future model inter-comparison studies explicitly examine the sensitivity of results to tropopause definition applied, including an emphasis toward online tropospheric ozone column calculations.

The ozone burden grows by approximately 40 % from PI (244 $\pm$ 30 Tg) to the PD (348 $\pm$ 15 Tg), and reaches a maximum of 402 $\pm$ 36 Tg in 2090. By year 2100, the burden is 396 $\pm$ 32 Tg, 60% above PI levels. The inter-model range varies across the integration, being 5 % for the PD, and 8-12% at the start and end of the period.

The ozone budget has been analysed in terms of ozone chemical production, loss, deposition, and the STE. Deposition, chemical ozone production and loss have been shown to increase steadily from the PI into the future, with the evolution of the ozone burden likely moderated by the behaviour of the stratospheric ozone burden. The variation in the growth rate of the ozone burden is shown to depend sensitively on the growth rate of emissions and the STE. There remains wider diversity between modelled ozone budget terms, with UKESM1 showing the largest fluxes, particularly in net chemical production, and the smallest STE.

At the start and end of the model period, inter-model diversity appears to be governed by biogenic VOCs. In contrast to the prescribed anthropogenic NO_x and CO emissions, emission fluxes of BVOCs are calculated online, as a function of environmental parameters. There is considerable variation in BVOC emissions across the models, and in the PI, UKESM1, the model with the highest ozone burden, has the largest emissions of BVOCs. The sensitivity of ozone production to NO_x

https://doi.org/10.5194/acp-2019-1216
Preprint. Discussion started: 10 February 2020

emissions has been calculated in the form of ozone production efficiency. This is also different across the three models, as it depends on VOC amounts and underpinning chemical mechanism. OPE, which is large in the PI, reaches a minimum around the PD, before recovering again into the later part of the 21st century. Again the model with the highest BVOC emissions in 2100, CESM2-WACCM, has the largest ozone burden. The dramatic increase in BVOC in this model, with the accompanying modest increase in ozone burden, underscores the importance of NO_x emissions as a controlling factor. Nevertheless, this analysis highlights the importance of BVOC in calculating the ozone response to anthropogenic NO_x and VOC emissions, and that accurate knowledge of future BVOC emissions is critical for our understanding of tropospheric ozone and its radiative forcing. The intermodel spread varies across the models, and becomes greater as we move away from simulation of present day conditions. The integrations reinforce the need for improvement to our process-level understanding of pre-industrial emissions of NO_x, particularly LNO_x and BVOCs, and of the climate-related factors that control future BVOC emissions.

The impact of the stratosphere on tropospheric ozone burden has been demonstrated. We find that STE fluxes are similar among the models in the PI, but that the STE evolves differently in the three models: UKESM1 has the largest ozone depletion in both hemispheres, whereas in CESM2-WACCM and GFDL-ESM4 there are ozone increases in the lower stratosphere northern high latitudes; this goes along with the inferred STE being very low in UKESM1 which may contribute to the smallest ozone burden trend in this model. Differences in stratospheric ozone in the models contribute significantly to the model spread in diagnosing ozone budget.

Stratospheric ozone depletion and recovery to tropospheric ozone has the biggest effect on the budget calculations around the year 2000. In this period, the decline in stratospheric ozone, and presumably STE, offsets a significant increase in net chemical ozone production over the period 1980-2000, which partially mitigates the response of tropospheric ozone to rapidly increasing emissions. The tropospheric burden over this period is therefore lower than it might otherwise have been, although the precise level of offset requires further clarification.

There remains a need to assess these future changes at the regional scale, and to understand which regions of the troposphere are most affected by future stratospheric ozone changes.

Data availability. Data used for this study were obtained from ESGF on November 28th, 2019.

Author contributions. PTG and LTM contriubted equally to this project. GZ, LTM, PTG, PJY, YMS, IG, DT, JL, OM provided data analysis and contributed to the writing and discussion of this manuscript; VN, PZ, ATA, LWH, OW, JMK, FOC, BH, STT contributed to the writing and discussion.

Competing interests. The authors declare no competing interests.

https://doi.org/10.5194/acp-2019-1216
Preprint. Discussion started: 10 February 2020

Atmospheric Chemistry and Physics Discussions

Acknowledgements. This work used JASMIN, the UK collaborative data analysis facility. IG thanks Suzie Molloy CSIRO Australia and Owen Cooper NOAA USA for assistance with data. BH was supported by the European Union's Horizon 2020 Framework Programme for Research and Innovation "Coordinated Research in Earth Systems and Climate: Experiments, kNowledge, Dissemination and Outreach (CRESCENDO)" project under Grant Agreement No. 641816. GZ was supported by the NZ Government's Strategic Science Investment Fund (SSIF) through the NIWA programme CACV. We thank Suzie Molloy (CSIRO) and Owen Cooper (NOAA) for providing surface ozone data. We acknowledge the World Climate Research Programme, which, through its Working Group on Coupled Modelling, coordinated and promoted CMIP6. We thank the climate modeling groups for producing and making available their model output, the Earth System Grid Federation (ESGF) for archiving the data and providing access, and the multiple funding agencies who support CMIP6 and ESGF.

https://doi.org/10.5194/acp-2019-1216
Preprint. Discussion started: 10 February 2020

Atmospheric Chemistry and Physics Discussions

References

Akritidis, D., Pozzer, A., Zanis, P., Tyrlis, E., Škerlak, B., Sprenger, M., and Lelieveld, J.: On the role of tropopause folds in summertime tropospheric ozone over the eastern Mediterranean and the Middle East, Atmospheric Chemistry and Physics, 16, 14 025–14 039, https://doi.org/https://doi.org/10.5194/acp-16-14025-2016, https://www.atmos-chem-phys.net/16/14025/2016/, 2016.

Akritidis, D., Pozzer, A., and Zanis, P.: On the impact of future climate change on tropopause folds and tropospheric ozone, Atmospheric Chemistry and Physics, 19, 14 387–14 401, https://doi.org/https://doi.org/10.5194/acp-19-14387-2019, https://www.atmos-chem-phys.net/19/14387/2019/, 2019.

Archibald, A. T., O'Connor, F. M., Abraham, N. L., Archer-Nicholls, S., Chipperfield, M. P., Dalvi, M., Folberth, G. A., Dennison, F., Dhomse, S. S., Griffiths, P. T., Hardacre, C., Hewitt, A. J., Hill, R., Johnson, C. E., Keeble, J., Köhler, M. O., Morgenstern, O., Mulchay, J. P., Ordóñez, C., Pope, R. J., Rumbold, S., Russo, M. R., Savage, N., Sellar, A., Stringer, M., Turnock, S., Wild, O., and Zeng, G.: Description and evaluation of the UKCA stratosphere-troposphere chemistry scheme (StratTrop vn 1.0) implemented in UKESM1, Geoscientific Model Development Discussions, 2019, 1–82, https://doi.org/10.5194/gmd-2019-246, https://www.geosci-model-dev-discuss.net/gmd-2019-246/, 2019.

Austin, J., Horowitz, L. W., Schwarzkopf, M. D., Wilson, R. J., and Levy, H.: Stratospheric Ozone and Temperature Simulated from the Preindustrial Era to the Present Day, Journal of Climate, 26, 3528–3543, https://doi.org/10.1175/JCLI-D-12-00162.1, https://journals.ametsoc.org/doi/full/10.1175/JCLI-D-12-00162.1, 2012.

Ayers, G. P., Penkett, S. A., Gillett, R. W., Bandy, B., Galbally, I. E., Meyer, C. P., Elsworth, C. M., Bentley, S. T., and Forgan, B. W.: Evidence for photochemical control of ozone concentrations in unpolluted marine air, Nature, 360, 446–449, https://doi.org/10.1038/360446a0, 1992.

Banerjee, A., Maycock, A. C., Archibald, A. T., Abraham, N. L., Telford, P., Braesicke, P., and Pyle, J. A.: Drivers of changes in stratospheric and tropospheric ozone between year 2000 and 2100, Atmospheric Chemistry and Physics, 16, 2727–2746, https://doi.org/10.5194/acp-16-2727-2016, https://www.atmos-chem-phys.net/16/2727/2016/, 2016.

Brewer, A. W. and Milford, J. R.: The Oxford-Kew ozone sonde, Proc. R. Soc. Lond. A, 256, 470–495, https://doi.org/10.1098/rspa.1960.0120, 1960.

Butchart, N.: The Brewer-Dobson circulation, Reviews of Geophysics, 52, 157–184, https://doi.org/10.1002/2013RG000448, https://agupubs.onlinelibrary.wiley.com/doi/abs/10.1002/2013RG000448, 2014.

Cooper, O. R., Parrish, D. D., Ziemke, J., Balashov, N. V., Cupeiro, M., Galbally, I. E., Gilge, S., Horowitz, L., Jensen, N. R., Lamarque, J.-F., Naik, V., Oltmans, S. J., Schwab, J., Shindell, D. T., Thompson, A. M., Thouret, V., Wang, Y., and Zbinden, R. M.: Global distribution and trends of tropospheric ozone: An observation-based review, Elem Sci Anth, 2, 000 029, https://doi.org/10.12952/journal.elementa.000029, http://www.elementascience.org/articles/10.12952/journal.elementa.000029/, 2014.

Danabasoglu, G.: NCAR CESM2-WACCM model output prepared for CMIP6 CMIP historical, https://doi.org/10.22033/ESGF/CMIP6.10071, https://doi.org/10.22033/ESGF/CMIP6.10071, 2019a.

Danabasoglu, G.: NCAR CESM2-WACCM model output prepared for CMIP6 ScenarioMIP, https://doi.org/10.22033/ESGF/CMIP6.10026, http://cera-www.dkrz.de/WDCC/meta/CMIP6/CMIP6.ScenarioMIP.NCAR.CESM2-WACCM, 2019b.

Danabasoglu, G., Bates, S. C., Briegleb, B. P., Jayne, S. R., Jochum, M., Large, W. G., Peacock, S., and Yeager, S. G.: The CCSM4 Ocean Component, Journal of Climate, 25, 1361–1389, https://doi.org/10.1175/JCLI-D-11-00091.1, https://doi.org/10.1175/JCLI-D-11-00091.1, 2012.

https://doi.org/10.5194/acp-2019-1216
Preprint. Discussion started: 10 February 2020

Atmospheric Chemistry and Physics Discussions

Doherty, R. M., Wild, O., Shindell, D. T., Zeng, G., MacKenzie, I. A., Collins, W. J., Fiore, A. M., Stevenson, D. S., Dentener, F. J., Schultz, M. G., Hess, P., Derwent, R. G., and Keating, T. J.: Impacts of climate change on surface ozone and intercontinental ozone pollution: A multi-model study, Journal of Geophysical Research: Atmospheres, 118, 3744–3763, https://doi.org/10.1002/jgrd.50266, https://agupubs.onlinelibrary.wiley.com/doi/abs/10.1002/jgrd.50266, 2013.

Draxler, R. R. and Hess, G. D.: Description of the HYSPLIT_4 modeling system, Tech. Rep. NOAA Technical Memorandum ERL ARL-224, NOAA ERL, 1997.

Draxler, R. R. and Hess, G. D.: An overview of the HYSPLIT_4 modeling system for trajectories, dispersion, and deposition, Australian Meteorology Magazine, 47, 295–308, 1998.

Dunne, J. et al.: The GFDL Earth System Model version 4.1 (GFDL-ESM4.1): Model description and simulation characteristics, Journal of Advances in Modeling Earth Systems., 4, 201–213, 2019.

Emmons, L. K., Orlando, J. J., Tyndall, G., Schwantes, R. H., Kinnison, D., Lamarque, J. F., Marsh, D., Mills, M., Tilmes, S., Buchholtz, R. R., Gettelman, A., Garcia, R., Simpson, I., Blake, D. R., and Pétron, G.: The Chemistry Mechanism in the Community Earth System Model version 2 (CESM2), In prep., 2019.

Eyring, V., Bony, S., Meehl, G. A., Senior, C. A., Stevens, B., Stouffer, R. J., and Taylor, K. E.: Overview of the Coupled Model Intercomparison Project Phase 6 (CMIP6) experimental design and organization, Geoscientific Model Development, 9, 1937–1958, https://doi.org/https://doi.org/10.5194/gmd-9-1937-2016, https://www.geosci-model-dev.net/9/1937/2016/, 2016.

Fiore, A. M., Naik, V., Spracklen, D. V., Steiner, A., Unger, N., Prather, M., Bergmann, D., Cameron-Smith, P. J., Cionni, I., Collins, W. J., Dalsøren, S., Eyring, V., Folberth, G. A., Ginoux, P., Horowitz, L. W., Josse, B., Lamarque, J.-F., MacKenzie, I. A., Nagashima, T., O'Connor, F. M., Righi, M., Rumbold, S. T., Shindell, D. T., Skeie, R. B., Sudo, K., Szopa, S., Takemura, T., and Zeng, G.: Global air quality and climate, Chemical Society Reviews, 41, 6663–6683, https://doi.org/10.1039/C2CS35095E, https://pubs.rsc.org/en/content/articlelanding/2012/cs/c2cs35095e, 2012.

Fiore, A. M., Naik, V., and Leibensperger, E. M.: Air Quality and Climate Connections, Journal of the Air & Waste Management Association, 65, 645–685, https://doi.org/10.1080/10962247.2015.1040526, https://doi.org/10.1080/10962247.2015.1040526, pMID: 25976481, 2015.

Fishman, J., Watson, C. E., Larsen, J. C., and Logan, J. A.: Distribution of tropospheric ozone determined from satellite data, J Geophys Res, 95, 3599–3617, https://doi.org/10.1029/JD095iD04p03599, 1990.

Fishman, J., Fakhruzzaman, K., Cros, B., and Nganga, D.: Identification of Widespread Pollution in the Southern Hemisphere Deduced from Satellite Analyses, Science, 252, 1693–1696, https://doi.org/10.1126/science.252.5013.1693, 1991.

Forster, P. M. d. F. and Shine, K. P.: Radiative forcing and temperature trends from stratospheric ozone changes, J Geophys Res, 102, 10 841–10 855, https://doi.org/10.1029/96JD03510, 1997.

Fountoukis, C. and Nenes, A.: ISORROPIA II: a computationally efficient thermodynamic equilibrium model for aerosols, Atmospheric Chemistry and Physics, 7, 4639–4659, https://doi.org/10.5194/acp-7-4639-2007, https://www.atmos-chem-phys.net/7/4639/2007/, 2007.

Fowler, D., Pilegaard, K., Sutton, M. A., Ambus, P., Raivonen, M., Duyzer, J., Simpson, D., Fagerli, H., Fuzzi, S., Schjoerring, J. K., Granier, C., Neftel, A., Isaksen, I. S. A., Laj, P., Maione, M., Monks, P. S., Burkhardt, J., Daemmgen, U., Neirynck, J., Personne, E., Wichink-Kruit, R., Butterbach-Bahl, K., Flechard, C., Tuovinen, J. P., Coyle, M., Gerosa, G., Loubet, B., Altimir, N., Gruenhage, L., Ammann, C., Cieslik, S., Paoletti, E., Mikkelsen, T. N., Ro-Poulsen, H., Cellier, P., Cape, J. N., Horváth, L., Loreto, F., Niinemets, U., Palmer, P. I., Rinne, J., Misztal, P., Nemitz, E., Nilsson, D., Pryor, S., Gallagher, M. W., Vesala, T., Skiba, U., Brüggemann, N., Zechmeister-Boltenstern, S., Williams, J., O'Dowd, C., Facchini, M. C., de Leeuw, G., Flossman, A., Chaumerliac, N., and

https://doi.org/10.5194/acp-2019-1216
Preprint. Discussion started: 10 February 2020

Erisman, J. W.: Atmospheric composition change: Ecosystems–Atmosphere interactions, Atmospheric Environment, 43, 5193–5267, https://doi.org/10.1016/j.atmosenv.2009.07.068, http://www.sciencedirect.com/science/article/pii/S1352231009006633, 2009.

Garcia, R. R. and Randel, W. J.: Acceleration of the Brewer–Dobson Circulation due to Increases in Greenhouse Gases, J Atmos Sci, 65, 2731–2739, https://doi.org/10.1175/2008JAS2712.1, 2008.

Gaudel, A., Cooper, O. R., Ancellet, G., Barret, B., Boynard, A., Burrows, J. P., Clerbaux, C., Coheur, P.-F., Cuesta, J., Cuevas, E., Doniki, S., Dufour, G., Ebojie, F., Foret, G., Garcia, O., Muños, M. J. G., Hannigan, J. W., Hase, F., Huang, G., Hassler, B., Hurtmans, D., Jaffe, D., Jones, N., Kalabokas, P., Kerridge, B., Kulawik, S. S., Latter, B., Leblanc, T., Flochmoën, E. L., Lin, W., Liu, J., Liu, X., Mahieu, E., McClure-Begley, A., Neu, J. L., Osman, M., Palm, M., Petetin, H., Petropavlovskikh, I., Querel, R., Rahpoe, N., Rozanov, A., Schultz, M. G., Schwab, J., Siddans, R., Smale, D., Steinbacher, M., Tanimoto, H., Tarasick, D. W., Thouret, V., Thompson, A. M., Trickl, T., Weatherhead, E., Wespes, C., Worden, H. M., Vigouroux, C., Xu, X., Zeng, G., and Ziemke, J.: Tropospheric Ozone Assessment Report: Present-day distribution and trends of tropospheric ozone relevant to climate and global atmospheric chemistry model evaluation, Elem Sci Anth, 6, 39, https://doi.org/10.1525/elementa.291, http://www.elementascience.org/articles/10.1525/elementa.291/, 2018.

Gettelman, A., Hannay, C., Bacmeister, J. T., Neale, R. B., Pendergrass, A. G., Danabasoglu, G., Lamarque, J.-F., Fasullo, J. T., Bailey, D. A., Lawrence, D. M., and Mills, M. J.: High Climate Sensitivity in the Community Earth System Model Version 2 (CESM2), Geophysical Research Letters, 46, 8329–8337, https://doi.org/10.1029/2019GL083978, https://agupubs.onlinelibrary.wiley.com/doi/abs/10.1029/2019GL083978, 2019.

Good, P., Sellar, A., Tang, Y., Rumbold, S., Ellis, R., Kelley, D., Kuhlbrodt, T., and Walton, J.: MOHC UKESM1.0-LL model output prepared for CMIP6 ScenarioMIP, https://doi.org/10.22033/ESGF/CMIP6.1567, http://cera-www.dkrz.de/WDCC/meta/CMIP6/CMIP6.ScenarioMIP.MOHC.UKESM1-0-LL, 2019.

Guenther, A., Karl, T., Harley, P., Wiedinmyer, C., Palmer, P. I., and Geron, C.: Estimates of global terrestrial isoprene emissions using MEGAN (Model of Emissions of Gases and Aerosols from Nature), Atmospheric Chemistry and Physics, 6, 3181–3210, https://doi.org/10.5194/acp-6-3181-2006, https://www.atmos-chem-phys.net/6/3181/2006/, 2006.

Guenther, A. B., Jiang, X., Heald, C. L., Sakulyanontvittaya, T., Duhl, T., Emmons, L. K., and Wang, X.: The Model of Emissions of Gases and Aerosols from Nature version 2.1 (MEGAN2.1): an extended and updated framework for modeling biogenic emissions, Geoscientific Model Development, 5, 1471–1492, https://doi.org/10.5194/gmd-5-1471-2012, https://www.geosci-model-dev.net/5/1471/2012/, 2012.

Hardacre, C., Wild, O., and Emberson, L.: An evaluation of ozone dry deposition in global scale chemistry climate models, Atmospheric Chemistry and Physics, 15, 6419–6436, https://doi.org/10.5194/acp-15-6419-2015, https://www.atmos-chem-phys.net/15/6419/2015/, 2015.

Helmig, D., Ganzeveld, L., Butler, T., and Oltmans, S. J.: The role of ozone atmosphere-snow gas exchange on polar, boundary-layer tropospheric ozone – a review and sensitivity analysis, Atmospheric Chemistry and Physics, 7, 15–30, https://doi.org/https://doi.org/10.5194/acp-7-15-2007, https://www.atmos-chem-phys.net/7/15/2007/, 2007.

Hodzic, A., Kasibhatla, P. S., Jo, D. S., Cappa, C. D., Jimenez, J. L., Madronich, S., and Park, R. J.: Rethinking the global secondary organic aerosol (SOA) budget: stronger production, faster removal, shorter lifetime, Atmospheric Chemistry and Physics, 16, 7917–7941, https://doi.org/10.5194/acp-16-7917-2016, https://www.atmos-chem-phys.net/16/7917/2016/, 2016.

Hoesly, R. M., Smith, S. J., Feng, L., Klimont, Z., Janssens-Maenhout, G., Pitkanen, T., Seibert, J. J., Vu, L., Andres, R. J., Bolt, R. M., Bond, T. C., Dawidowski, L., Kholod, N., Kurokawa, J.-I., Li, M., Liu, L., Lu, Z., Moura, M. C. P., O'Rourke, P. R., and Zhang, Q.: Historical (1750–2014) anthropogenic emissions of reactive gases and aerosols from the Community Emissions Data System (CEDS), Geoscientific Model Development, 11, 369–408, https://doi.org/10.5194/gmd-11-369-2018, https://www.geosci-model-dev.net/11/369/2018/, 2018.

https://doi.org/10.5194/acp-2019-1216
Preprint. Discussion started: 10 February 2020

Atmospheric Chemistry and Physics Discussions

Horowitz, L. W., V, Naik, F., Paulot, P. A., Ginoux, J. P., Dunne, J., Mao, J., Schnell, J., Chen, X., Lin, M., Lin, P., Malyshev, S., Paynter, D., Shevliakova, E., and Zhao, M.: The GFDL Global Atmospheric Chemistry-Climate Model AM4.1: Model Description and Simulation Characteristics., submitted to Journal of Advances in Modeling Earth Systems, 2019.

Hu, L., Jacob, D. J., Liu, X., Zhang, Y., Zhang, L., Kim, P. S., Sulprizio, M. P., and Yantosca, R. M.: Global budget of tropospheric ozone: Evaluating recent model advances with satellite (OMI), aircraft (IAGOS), and ozonesonde observations, Atmospheric Environment, 167, 323–334, https://doi.org/10.1016/j.atmosenv.2017.08.036, http://www.sciencedirect.com/science/article/pii/S1352231017305484, 2017.

Hunke, E., Lipscomb, W., Turner, A., Jeffery, N., and Elliott, S.: CICE: The Los Alamos Sea ice Model Documentation and Software User's Manual Version 5 (Tech. Rep. LA-CC-06–012), Los Alamos, NM: Los Alamos National Laboratory, 2015.

Jerrett, M., Burnett, R. T., Pope, C. A., Ito, K., Thurston, G., Krewski, D., Shi, Y., Calle, E., and Thun, M.: Long-Term Ozone Exposure and Mortality, New England Journal of Medicine, 360, 1085–1095, https://doi.org/10.1056/NEJMoa0803894, https://doi.org/10.1056/NEJMoa0803894, 2009.

John, J. G., Blanton, C., McHugh, C., Nikonov, S., Radhakrishnan, A., Rand, K., Vahlenkamp, H., Zadeh, N. T., Gauthier, P. P., Ginoux, P., Harrison, M., Horowitz, L. W., Malyshev, S., Naik, V., Paynter, D. J., Ploshay, J., Silvers, L., Stock, C., Winton, M., Zeng, Y., and Dunne, J. P.: NOAA-GFDL GFDL-ESM4 model output prepared for CMIP6 ScenarioMIP, https://doi.org/10.22033/ESGF/CMIP6.1414, http://cera-www.dkrz.de/WDCC/meta/CMIP6/CMIP6.ScenarioMIP.NOAA-GFDL.GFDL-ESM4, 2018.

Johnson, C. E., Collins, W. J., Stevenson, D. S., and Derwent, R. G.: Relative roles of climate and emissions changes on future tropospheric oxidant concentrations, Journal of Geophysical Research: Atmospheres, 104, 18 631–18 645, https://doi.org/10.1029/1999JD900204, https://agupubs.onlinelibrary.wiley.com/doi/abs/10.1029/1999JD900204, 1999.

Karset, I. H. H., Berntsen, T. K., Storelvmo, T., Alterskjær, K., Grini, A., Olivie, D., Kirkevag, A., Seland, O., Iversen, T., and Schulz, M.: Strong impacts on aerosol indirect effects from historical oxidant changes, Atmospheric Chemistry and Physics, 18, 7669–7690, https://doi.org/https://doi.org/10.5194/acp-18-7669-2018, https://www.atmos-chem-phys.net/18/7669/2018/, 2018.

Katragkou, E., Zanis, P., Tsikerdekis, A., Kapsomenakis, J., Melas, D., Eskes, H., Flemming, J., Huijnen, V., Inness, A., Schultz, M. G., Stein, O., and Zerefos, C. S.: Evaluation of near-surface ozone over Europe from the MACC reanalysis, Geoscientific Model Development, 8, 2299–2314, https://doi.org/https://doi.org/10.5194/gmd-8-2299-2015, https://www.geosci-model-dev.net/8/2299/2015/, 2015.

Kelley, M., Schmidt, G. A., Nazarenko, L., Miller, R. L., Bauer, S. E., Ruedy, R., Russell, G. L., Aleinov, I., Bauer, M., Bleck, R., Canuto, V., Cesana, G., Cheng, Y., Clune, T. L., Cook, B., Cruz, C. A., Del Genio, A. D., Elsaesser, G. S., Faluvegi, G., Kiang, N. Y., Kim, D., Lacis, A. A., Leboissetier, A., LeGrande, A. N., Lo, K. K., Marshall, J. C., McDermid, S., Matthews, E. E., Mezuman, K., Murray, L. T., Oinas, V., Orbe, C., Pérez García-Pando, C., Perlwitz, J. P., Puma, M. J., Rind, D., Romanou, A., Shindell, D. T., Sun, S., Tausnev, N., Tsigaridis, K., Tselioudis, G., Weng, E., Wu, J., and Yao, M.-S.: GISS-E2.1: Configurations and Climatology, submitted to J Adv Model Earth Sy, 2019.

Kerr, J. B., Fast, H., McElroy, C. T., Oltmans, S. J., Lathrop, J. A., Kyro, E., Paukkunen, A., Claude, H., Köhler, U., Sreedharan, C. R., Takao, T., and Tsukagoshi, Y.: The 1991 WMO International ozonesonde intercomparison at Vanscoy, Canada, Atmos Ocean, 32, 685–716, https://doi.org/10.1080/07055900.1994.9649518, 1994.

Koch, D. M., Schmidt, G. A., and Field, C. V.: Sulfur, sea salt, and radionuclide aerosols in GISS ModelE, J Geophys Res, 111, D06 206, https://doi.org/10.1029/2004JD005550, 2006.

Komhyr, W. D.: Electrochemical Concentration Cells for Gas Analysis, Ann Géophys, 25, 203, 1969.

Komhyr, W. D.: Development of an ECC-Ozonesonde, Tech. Rep. NOAA Techn. Rep. ERL 200-APCL 18ARL-149, NOAA ERL, 1971.

https://doi.org/10.5194/acp-2019-1216
Preprint. Discussion started: 10 February 2020

Krasting, J. P., John, J. G., Blanton, C., McHugh, C., Nikonov, S., Radhakrishnan, A., Rand, K., Zadeh, N. T., Balaji, V., Durachta, J., Dupuis, C., Menzel, R., Robinson, T., Underwood, S., Vahlenkamp, H., Dunne, K. A., Gauthier, P. P., Ginoux, P., Griffies, S. M., Hallberg, R., Harrison, M., Hurlin, W., Malyshev, S., Naik, V., Paulot, F., Paynter, D. J., Ploshay, J., Schwarzkopf, D. M., Seman, C. J., Silvers, L., Wyman, B., Zeng, Y., Adcroft, A., Dunne, J. P., Guo, H., Held, I. M., Horowitz, L. W., Milly, P., Shevliakova, E., Stock, C., Winton, M., and Zhao, M.: NOAA-GFDL GFDL-ESM4 model output prepared for CMIP6 CMIP historical, https://doi.org/10.22033/ESGF/CMIP6.8597, http://cera-www.dkrz.de/WDCC/meta/CMIP6/CMIP6.CMIP.NOAA-GFDL.GFDL-ESM4.historical, 2018.

Lipscomb, W. H., Price, S. F., Hoffman, M. J., Leguy, G. R., Bennett, A. R., Bradley, S. L., Evans, K. J., Fyke, J. G., Kennedy, J. H., Perego, M., Ranken, D. M., Sacks, W. J., Salinger, A. G., Vargo, L. J., and Worley, P. H.: Description and evaluation of the Community Ice Sheet Model (CISM) v2.1, Geoscientific Model Development, 12, 387–424, https://doi.org/10.5194/gmd-12-387-2019, https://www.geosci-model-dev.net/12/387/2019/, 2019.

Liu, G., Liu, J., Tarasick, D. W., Fioletov, V. E., Jin, J. J., Moeini, O., Liu, X., Sioris, C. E., and Osman, M.: A global tropospheric ozone climatology from trajectory-mapped ozone soundings, Atmos Chem Phys, 13, 10 659–10 675, https://doi.org/10.5194/acp-13-10659-2013, 2013a.

Liu, J., Tarasick, D. W., Fioletov, V. E., McLinden, C., Zhao, T., Gong, S., Sioris, C., Jin, J. J., Liu, G., and Moeini, O.: A global ozone climatology from ozone soundings via trajectory mapping: a stratospheric perspective, Atmos Chem Phys, 13, 11 441–11 464, https://doi.org/10.5194/acp-13-11441-2013, 2013b.

Malley, C. S., Henze, D. K., Kuylenstierna, J. C., Vallack, H. W., Davila, Y., Anenberg, S. C., Turner, M. C., and Ashmore, M. R.: Updated Global Estimates of Respiratory Mortality in Adults $\geq$ 30Years of Age Attributable to Long-Term Ozone Exposure, Environmental Health Perspectives, 125, 087 021, https://doi.org/10.1289/EHP1390,https://doi.org/10.1289/EHP1390, https://ehp.niehs.nih.gov/doi/10.1289/EHP1390, 2017.

Meinshausen, M., Nicholls, Z., Lewis, J., Gidden, M. J., Vogel, E., Freund, M., Beyerle, U., Gessner, C., Nauels, A., Bauer, N., Canadell, J. G., Daniel, J. S., John, A., Krummel, P., Luderer, G., Meinshausen, N., Montzka, S. A., Rayner, P., Reimann, S., Smith, S. J., Berg, M. v. d., Velders, G. J. M., Vollmer, M., and Wang, H. J.: The SSP greenhouse gas concentrations and their extensions to 2500, Geoscientific Model Development Discussions, pp. 1–77, https://doi.org/https://doi.org/10.5194/gmd-2019-222, https://www.geosci-model-dev-discuss.net/gmd-2019-222/, 2019.

Meul, S., Langematz, U., Kröger, P., Oberländer-Hayn, S., and Jöckel, P.: Future changes in the stratosphere-to-troposphere ozone mass flux and the contribution from climate change and ozone recovery, Atmospheric Chemistry and Physics, 18, 7721–7738, https://doi.org/https://doi.org/10.5194/acp-18-7721-2018, https://www.atmos-chem-phys.net/18/7721/2018/acp-18-7721-2018.html, 2018.

Miller, R. L., Schmidt, G. A., Nazarenko, L., Bauer, S. E., Kelley, M., Ruedy, R., Russell, G. L., Aleinov, I., Bauer, M., Bleck, R., Canuto, V., Cesana, G., Cheng, Y., Clune, T. L., Cook, B., Cruz, C. A., Del Genio, A. D., Elsaesser, G. S., Faluvegi, G., Kiang, N. Y., Kim, D., Lacis, A. A., Leboissetier, A., LeGrande, A. N., Lo, K. K., Marshall, J. C., McDermid, S., Matthews, E. E., Mezuman, K., Murray, L. T., Oinas, V., Orbe, C., Pérez García-Pando, C., Perlwitz, J. P., Puma, M. J., Rind, D., Romanou, A., Shindell, D. T., Sun, S., Tausnev, N., Tsigaridis, K., Tselioudis, G., Weng, E., Wu, J., and Yao, M.-S.: CMIP6 historical simulations (1850-2014) with GISS ModelE2.1, submitted to J Adv Model Earth Sy, 2020.

Mills, M. J., Schmidt, A., Easter, R., Solomon, S., Kinnison, D. E., Ghan, S. J., Neely, R. R., Marsh, D. R., Conley, A., Bardeen, C. G., and Gettelman, A.: Global volcanic aerosol properties derived from emissions, 1990–2014, using CESM1(WACCM), Journal of Geophysi-

cal Research: Atmospheres, 121, 2332–2348, https://doi.org/10.1002/2015JD024290, https://agupubs.onlinelibrary.wiley.com/doi/abs/10.1002/2015JD024290, 2016.

Monks, P. S., Archibald, A. T., Colette, A., Cooper, O., Coyle, M., Derwent, R., Fowler, D., Granier, C., Law, K. S., Mills, G. E., Stevenson, D. S., Tarasova, O., Thouret, V., von Schneidemesser, E., Sommariva, R., Wild, O., and Williams, M. L.: Tropospheric ozone and its precursors from the urban to the global scale from air quality to short-lived climate forcer, Atmospheric Chemistry and Physics, 15, 8889–8973, https://doi.org/https://doi.org/10.5194/acp-15-8889-2015, https://www.atmos-chem-phys.net/15/8889/2015/, 2015.

Moore, J. K., Lindsay, K., Doney, S. C., Long, M. C., and Misumi, K.: Marine Ecosystem Dynamics and Biogeochemical Cycling in the Community Earth System Model [CESM1(BGC)]: Comparison of the 1990s with the 2090s under the RCP4.5 and RCP8.5 Scenarios, Journal of Climate, 26, 9291–9312, https://doi.org/10.1175/JCLI-D-12-00566.1, https://doi.org/10.1175/JCLI-D-12-00566.1, 2013.

Morgenstern, O., Braesicke, P., O'Connor, F. M., Bushell, A. C., Johnson, C. E., Osprey, S. M., and Pyle, J. A.: Evaluation of the new UKCA climate-composition model – Part 1: The stratosphere, Geoscientific Model Development, 2, 43–57, https://doi.org/https://doi.org/10.5194/gmd-2-43-2009, https://www.geosci-model-dev.net/2/43/2009/gmd-2-43-2009.html, 2009.

Morgenstern, O., Stone, K. A., Schofield, R., Akiyoshi, H., Yamashita, Y., Kinnison, D. E., Garcia, R. R., Sudo, K., Plummer, D. A., Scinocca, J., Oman, L. D., Manyin, M. E., Zeng, G., Rozanov, E., Stenke, A., Revell, L. E., Pitari, G., Mancini, E., Genova, G. D., Visioni, D., Dhomse, S. S., and Chipperfield, M. P.: Ozone sensitivity to varying greenhouse gases and ozone-depleting substances in CCMI-1 simulations, Atmospheric Chemistry and Physics, 18, 1091–1114, https://doi.org/https://doi.org/10.5194/acp-18-1091-2018, https://www.atmos-chem-phys.net/18/1091/2018/, 2018.

Mulcahy, J. P., Jones, C., Sellar, A., Johnson, B., Boutle, I. A., Jones, A., Andrews, T., Rumbold, S. T., Mollard, J., Bellouin, N., Johnson, C. E., Williams, K. D., Grosvenor, D. P., and McCoy, D. T.: Improved Aerosol Processes and Effective Radiative Forcing in HadGEM3 and UKESM1, Journal of Advances in Modeling Earth Systems, 10, 2786–2805, https://doi.org/10.1029/2018MS001464, https://agupubs.onlinelibrary.wiley.com/doi/abs/10.1029/2018MS001464, 2018.

Myhre, G., Shindell, D., Bréon, F.-M., Collins, W., Fuglestvedt, J., Huang, J., Koch, D., Lamarque, J.-F., Lee, D., Mendoza, B., Nakajima, T., Robock, A., Stephens, G., Takemura, T., and Zhang, H.: Anthropogenic and Natural Radiative Forcing, in: Climate Change 2013: The Physical Science Basis. Contribution of Working Group I to the Fifth Assessment Report of the Intergovernmental Panel on Climate Change, edited by Stocker, T., Qin, D., Plattner, G.-K., Tignor, M., Allen, S., Boschung, J., Nauels, A., Xia, Y., Bex, V., and Midgley, P., pp. 659–740, Cambridge University Press, Cambridge, United Kingdom and New York, NY, USA, https://doi.org/10.1017/CBO9781107415324.018, www.climatechange2013.org, 2013.

Naik, V., Horowitz, L. W., Fiore, A. M., Ginoux, P., Mao, J., Aghedo, A. M., and Levy, H.: Impact of preindustrial to present-day changes in short-lived pollutant emissions on atmospheric composition and climate forcing, Journal of Geophysical Research: Atmospheres, 118, 8086–8110, https://doi.org/10.1002/jgrd.50608, https://agupubs.onlinelibrary.wiley.com/doi/abs/10.1002/jgrd.50608, 2013.

NASA Goddard Institute For Space Studies (NASA/GISS): NASA-GISS GISS-E2-1-G-CC model output prepared for CMIP6 CMIP historical, https://doi.org/10.22033/ESGF/CMIP6.11762, http://cera-www.dkrz.de/WDCC/meta/CMIP6/CMIP6.CMIP.NASA-GISS.GISS-E2-1-G-CC.historical, 2019.

Oberländer-Hayn, S., Gerber, E. P., Abalichin, J., Akiyoshi, H., Kerschbaumer, A., Kubin, A., Kunze, M., Langematz, U., Meul, S., Michou, M., Morgenstern, O., and Oman, L. D.: Is the Brewer-Dobson circulation increasing or moving upward?, Geophysical Research Letters, 43, 1772–1779, https://doi.org/10.1002/2015GL067545, https://agupubs.onlinelibrary.wiley.com/doi/abs/10.1002/2015GL067545, 2016.

O'Connor, F. M., Johnson, C. E., Morgenstern, O., Abraham, N. L., Braesicke, P., Dalvi, M., Folberth, G. A., Sanderson, M. G., Telford, P. J., Voulgarakis, A., Young, P. J., Zeng, G., Collins, W. J., and Pyle, J. A.: Evaluation of the new UKCA climate-composition model. Part 2:

The Troposphere, Geoscientific Model Development, 7, 41–91, https://doi.org/10.5194/gmd-7-41-2014, https://www.geosci-model-dev.net/7/41/2014/, 2014.

Oltmans, S. J. and Levy, H.: Surface ozone measurements from a global network, Atmospheric Environment, 28, 9–24, https://doi.org/10.1016/1352-2310(94)90019-1, http://www.sciencedirect.com/science/article/pii/1352231094900191, 1994.

Pacifico, F., Harrison, S. P., Jones, C. D., Arneth, A., Sitch, S., Weedon, G. P., Barkley, M. P., Palmer, P. I., Serça, D., Potosnak, M., Fu, T.-M., Goldstein, A., Bai, J., and Schurgers, G.: Evaluation of a photosynthesis-based biogenic isoprene emission scheme in JULES and simulation of isoprene emissions under present-day climate conditions, Atmospheric Chemistry and Physics, 11, 4371–4389, https://doi.org/10.5194/acp-11-4371-2011, https://www.atmos-chem-phys.net/11/4371/2011/, 2011.

Polvani, L. M., Abalos, M., Garcia, R., Kinnison, D., and Randel, W. J.: Significant weakening of Brewer-Dobson circulation trends over the 21st century as a consequence of the Montreal Protocol, J. Geophys. Res., 45, 401–409, https://doi.org/10.1002/2017GL075345, 2018.

Polvani, L. M., Wang, L., Abalos, M., Butchart, N., Chipperfield, M. P., Dameris, M., Deushi, M., Dhomse, S. S., Jöcke, P., Kinnison, D., Michou, M., Morgenstern, O., Oman, L. D., Plummer, D. A., and Stone, K. A.: Large impacts, past and future, of ozone-depleting substances on Brewer-Dobson circulation trends: A multimodel assessment, J. Geophys. Res., 124, 6669–6680, https://doi.org/10.1029/2018JD029516, 2019.

Price, C. and Rind, D.: A simple lightning parameterization for calculating global lightning distributions, Journal of Geophysical Research: Atmospheres, 97, 9919–9933, https://doi.org/10.1029/92JD00719, https://agupubs.onlinelibrary.wiley.com/doi/abs/10.1029/92JD00719, 1992.

Price, C. and Rind, D.: What determines the cloud-to-ground lightning fraction in thunderstorms?, Geophysical Research Letters, 20, 463–466, https://doi.org/10.1029/93GL00226, https://agupubs.onlinelibrary.wiley.com/doi/abs/10.1029/93GL00226, 1993.

Revell, L. E., Tummon, F., Stenke, A., Sukhodolov, T., Coulon, A., Rozanov, E., Garny, H., Grewe, V., and Peter, T.: Drivers of the tropospheric ozone budget throughout the 21st century under the medium-high climate scenario RCP 6.0, Atmospheric Chemistry and Physics, 15, 5887–5902, https://doi.org/https://doi.org/10.5194/acp-15-5887-2015, https://www.atmos-chem-phys.net/15/5887/2015/, 2015.

Romanou, A., Gregg, W. W., Romanski, J., Kelley, M., Bleck, R., Healy, R., Nazarenko, L. S., Russell, G., Schmidt, G. A., Sun, S., and Tausnev, N.: Natural air–sea flux of CO2 in simulations of the NASA-GISS climate model: Sensitivity to the physical ocean model formulation, Ocean Model, 66, 26–44, https://doi.org/10.1016/j.ocemod.2013.01.008, 2013.

Rosenlof, K. H.: Seasonal cycle of the residual mean meridional circulation in the stratosphere, Journal of Geophysical Research: Atmospheres (1984–2012), 100, 5173–5191, https://doi.org/10.1029/94JD03122, 1995.

Sauvage, B., Thouret, V., Thompson, A. M., Witte, J. C., Cammas, J. P., Nedelec, P., and Athier, G.: Enhanced view of the "tropical Atlantic ozone paradox" and "zonal wave one" from the in situ MOZAIC and SHADOZ data, J Geophys Res, 111, D01 301, https://doi.org/10.1029/2005JD006241, 2006.

Sauvage, B., Martin, R. V., Donkelaar, A. v., and Ziemke, J. R.: Quantification of the factors controlling tropical tropospheric ozone and the South Atlantic maximum, Journal of Geophysical Research: Atmospheres, 112, https://doi.org/10.1029/2006JD008008, https://agupubs.onlinelibrary.wiley.com/doi/abs/10.1029/2006JD008008, 2007.

Schnell, J. L., Naik, V., Horowitz, L. W., Paulot, F., Mao, J., Ginoux, P., Zhao, M., and Ram, K.: Exploring the relationship between surface $PM_{2.5}$ and meteorology in Northern India, Atmospheric Chemistry and Physics, 18, 10 157–10 175, https://doi.org/10.5194/acp-18-10157-2018, https://www.atmos-chem-phys.net/18/10157/2018/, 2018.

https://doi.org/10.5194/acp-2019-1216
Preprint. Discussion started: 10 February 2020

Sekiya, T. and Sudo, K.: Roles of transport and chemistry processes in global ozone change on interannual and multidecadal time scales, Journal of Geophysical Research: Atmospheres, 119, 4903–4921, https://doi.org/10.1002/2013JD020838, https://agupubs.onlinelibrary.wiley.com/doi/abs/10.1002/2013JD020838, 2014.

Sellar, A. A., Jones, C. G., Mulcahy, J. P., Tang, Y., Yool, A., Wiltshire, A., O'Connor, F. M., Stringer, M., Hill, R., Palmieri, J., Woodward, S., Mora, L. d., Kuhlbrodt, T., Rumbold, S. T., Kelley, D. I., Ellis, R., Johnson, C. E., Walton, J., Abraham, N. L., Andrews, M. B., Andrews, T., Archibald, A. T., Berthou, S., Burke, E., Blockley, E., Carslaw, K., Dalvi, M., Edwards, J., Folberth, G. A., Gedney, N., Griffiths, P. T., Harper, A. B., Hendry, M. A., Hewitt, A. J., Johnson, B., Jones, A., Jones, C. D., Keeble, J., Liddicoat, S., Morgenstern, O., Parker, R. J., Predoi, V., Robertson, E., Siahaan, A., Smith, R. S., Swaminathan, R., Woodhouse, M. T., Zeng, G., and Zerroukat, M.: UKESM1: Description and Evaluation of the U.K. Earth System Model, Journal of Advances in Modeling Earth Systems, n/a, https://doi.org/10.1029/2019MS001739, https://agupubs.onlinelibrary.wiley.com/doi/abs/10.1029/2019MS001739, 2019.

Shindell, D. T., Grenfell, J. L., Rind, D. H., Grewe, V., and Price, C. G.: Chemistry-climate interactions in the Goddard Institute for Space Studies general circulation model: 1. Tropospheric chemistry model description and evaluation, J Geophys Res, 106, 8047, https://doi.org/10.1029/2000JD900704, 2001.

Shindell, D. T., Faluvegi, G., and Bell, N.: Preindustrial-to-present-day radiative forcing by tropospheric ozone from improved simulations with the GISS chemistry-climate GCM, Atmos Chem Phys, 3, 1675–1702, https://doi.org/10.5194/acp-3-1675-2003, 2003.

Shindell, D. T., Faluvegi, G., Unger, N., Aguilar, E., Schmidt, G. A., Koch, D. M., Bauer, S. E., and Miller, R. L.: Simulations of preindustrial, present-day, and 2100 conditions in the NASA GISS composition and climate model G-PUCCINI, Atmos Chem Phys, 6, 4427–4459, https://doi.org/10.5194/acp-6-4427-2006, 2006.

Shindell, D. T., Faluvegi, G., Koch, D. M., Schmidt, G. A., Unger, N., and Bauer, S. E.: Improved Attribution of Climate Forcing to Emissions, Science, 326, 716–718, https://doi.org/10.1126/science.1174760, http://science.sciencemag.org/content/326/5953/716, 2009.

Shindell, D. T., Pechony, O., Voulgarakis, A., Faluvegi, G., Nazarenko, L. S., Lamarque, J.-F., Bowman, K. W., Milly, G., Kovari, B., Ruedy, R., and Schmidt, G. A.: Interactive ozone and methane chemistry in GISS-E2 historical and future climate simulations, Atmos Chem Phys, 13, 2653–2689, https://doi.org/10.5194/acp-13-2653-2013, 2013.

Shiotani, M.: Annual, quasi-biennial, and El Niño-Southern Oscillation (ENSO)time-scale variations in equatorial total ozone, J Geophys Res, 97, 7625–7633, https://doi.org/10.1029/92JD00530, 1992.

Sitch, S., Cox, P. M., Collins, W. J., and Huntingford, C.: Indirect radiative forcing of climate change through ozone effects on the land-carbon sink, Nature, 448, 791–794, https://doi.org/10.1038/nature06059, https://www.nature.com/articles/nature06059, 2007.

Smit, H. G. J., Straeter, W., Johnson, B. J., Oltmans, S. J., Davies, J., Tarasick, D. W., Hoegger, B., Stübi, R., Schmidlin, F. J., Northam, T., Thompson, A. M., Witte, J. C., Boyd, I., and Posny, F.: Assessment of the performance of ECC-ozonesondes under quasi-flight conditions in the environmental simulation chamber: Insights from the Juelich Ozone Sonde Intercomparison Experiment (JOSIE), J Geophys Res, 112, 563, https://doi.org/10.1029/2006JD007308, 2007.

Smith, R. and Gent, P.: Reference manual for the Parallel Ocean Program (POP), ocean component of the Community Climate System Model (CCSM2.0), Los Alamos National Laboratory Technical Report, 2002.

Stevenson, D. S., Dentener, F. J., Schultz, M. G., Ellingsen, K., van Noije, T. P. C., Wild, O., Zeng, G., Amann, M., Atherton, C. S., Bell, N., Bergmann, D. J., Bey, I., Butler, T., Cofala, J., Collins, W. J., Derwent, R. G., Doherty, R. M., Drevet, J., Eskes, H. J., Fiore, A. M., Gauss, M., Hauglustaine, D. A., Horowitz, L. W., Isaksen, I. S. A., Krol, M. C., Lamarque, J.-F., Lawrence, M. G., Montanaro, V., Muller, J. F., Pitari, G., Prather, M. J., Pyle, J. A., Rast, S., Rodriguez, J. M., Sanderson, M. G., Savage, N. H., Shindell, D. T., Strahan, S. E., Sudo,

https://doi.org/10.5194/acp-2019-1216
Preprint. Discussion started: 10 February 2020

K., and Szopa, S.: Multimodel ensemble simulations of present-day and near-future tropospheric ozone, J Geophys Res, 111, D08 301, https://doi.org/10.1029/2005JD006338, 2006.

Stevenson, D. S., Young, P. J., Naik, V., Lamarque, J.-F., Shindell, D. T., Voulgarakis, A., Skeie, R. B., Dalsoren, S. B., Myhre, G., Berntsen, T. K., Folberth, G. A., Rumbold, S. T., Collins, W. J., MacKenzie, I. A., Doherty, R. M., Zeng, G., Noije, T. P. C. v., Strunk, A., Bergmann, D., Cameron-Smith, P., Plummer, D. A., Strode, S. A., Horowitz, L., Lee, Y. H., Szopa, S., Sudo, K., Nagashima, T., Josse, B., Cionni, I., Righi, M., Eyring, V., Conley, A., Bowman, K. W., Wild, O., and Archibald, A.: Tropospheric ozone changes, radiative forcing and attribution to emissions in the Atmospheric Chemistry and Climate Model Intercomparison Project (ACCMIP), Atmospheric Chemistry and Physics, 13, 3063–3085, https://doi.org/https://doi.org/10.5194/acp-13-3063-2013, https://www.atmos-chem-phys.net/13/3063/2013/, 2013.

Sun, S. and Bleck, R.: Multi-century simulations with the coupled GISS–HYCOM climate model: control experiments, Clim Dynam, 26, 407–428, https://doi.org/10.1007/s00382-005-0091-7, 2006.

Tang, Y., Rumbold, S., Ellis, R., Kelley, D., Mulcahy, J., Sellar, A., Walton, J., and Jones, C.: MOHC UKESM1.0-LL model output prepared for CMIP6 CMIP historical, https://doi.org/10.22033/ESGF/CMIP6.6113, http://cera-www.dkrz.de/WDCC/meta/CMIP6/CMIP6.CMIP.MOHC.UKESM1-0-LL.historical, 2019.

Tarasick, D., Galbally, I. E., Cooper, O. R., Schultz, M. G., Ancellet, G., Leblanc, T., Wallington, T. J., Ziemke, J. R., Liu, X., Steinbacher, M., Staehelin, J., Vigouroux, C., Hannigan, J. W., García, O., Foret, G., Zanis, P., Weatherhead, E., Petropavlovskikh, I., Worden, H. M., Osman, M., Liu, J. J., Chang, K.-L., Gaudel, A., Lin, M., Granados-Muñoz, M., Thompson, A. M., Oltmans, S. J., Cuesta, J., Dufour, G., Thouret, V., Hassler, B., Trickl, T., and Neu, J. L.: Tropospheric Ozone Assessment Report: Tropospheric ozone from 1877 to 2016, observed levels, trends and uncertainties, Elem Sci Anth, 7, 39, https://doi.org/10.1525/elementa.376, 2019.

Tarasick, D. W., Jin, J. J., Fioletov, V. E., Liu, G., Thompson, A. M., Oltmans, S. J., Liu, J., Sioris, C. E., Liu, X., Cooper, O. R., Dann, T., and Thouret, V.: High-resolution tropospheric ozone fields for INTEX and ARCTAS from IONS ozonesondes, J Geophys Res, 115, D12S15, https://doi.org/10.1029/2009JD012918, 2010.

Tarasick, D. W., Davies, J., Smit, H. G. J., and Oltmans, S. J.: A re-evaluated Canadian ozonesonde record: measurements of the vertical distribution of ozone over Canada from 1966 to 2013, Atmos Meas Tech, 9, 195–214, https://doi.org/10.5194/amt-9-195-2016, 2016.

Thompson, A. M.: Southern Hemisphere Additional Ozonesondes (SHADOZ) 1998–2000 tropical ozone climatology 1. Comparison with Total Ozone Mapping Spectrometer (TOMS) and ground-based measurements, J Geophys Res, 108, 8238, https://doi.org/10.1029/2001JD000967, 2003a.

Thompson, A. M.: Southern Hemisphere Additional Ozonesondes (SHADOZ) 1998–2000 tropical ozone climatology 2. Tropospheric variability and the zonal wave-one, J Geophys Res, 108, 8241, https://doi.org/10.1029/2002JD002241, 2003b.

Thompson, A. M. and Hudson, R. D.: Tropical tropospheric ozone (TTO) maps from Nimbus 7 and Earth Probe TOMS by the modified-residual method: Evaluation with sondes, ENSO signals, and trends from Atlantic regional time series, J Geophys Res, 104, 26 961, https://doi.org/10.1029/1999JD900470, 1999.

Thompson, A. M., Doddridge, B. G., Witte, J. C., Hudson, R. D., Luke, W. T., Johnson, J. E., Johnson, B. J., Oltmans, S. J., and Weller, R.: A tropical Atlantic Paradox: Shipboard and satellite views of a tropospheric ozone maximum and wave-one in January-February 1999, Geophys Res Lett, 27, 3317–3320, https://doi.org/10.1029/1999GL011273, 2000.

Tilmes, S.and Hodzic, A., and, J., J., K., Mills, J., M., Gettelman, A., Kinnison, D., Park, M., Lamarque, J.-F., Vitt, F., Shrivastava, P., Campuzano, J., Jimenez, J., and Liu, X.: Climate forcing and trends of organic aerosols in the Community Earth System Model (CESM2), Manuscript submitted for publication., 2019.

https://doi.org/10.5194/acp-2019-1216
Preprint. Discussion started: 10 February 2020

Tilmes, S., Lamarque, J.-F., Emmons, L. K., Kinnison, D. E., Marsh, D., Garcia, R. R., Smith, A. K., Neely, R. R., Conley, A., Vitt, F., Val Martin, M., Tanimoto, H., Simpson, I., Blake, D. R., and Blake, N.: Representation of the Community Earth System Model (CESM1) CAM4-chem within the Chemistry-Climate Model Initiative (CCMI), Geoscientific Model Development, 9, 1853–1890, https://doi.org/https://doi.org/10.5194/gmd-9-1853-2016, https://www.geosci-model-dev.net/9/1853/2016/, 2016.

Turner, M. C., Jerrett, M., Pope, C. A., Krewski, D., Gapstur, S. M., Diver, W. R., Beckerman, B. S., Marshall, J. D., Su, J., Crouse, D. L., and Burnett, R. T.: Long-Term Ozone Exposure and Mortality in a Large Prospective Study, American Journal of Respiratory and Critical Care Medicine, 193, 1134–1142, https://doi.org/10.1164/rccm.201508-1633OC, https://www.atsjournals.org/doi/10.1164/rccm.201508-1633OC, 2015.

Turnock, S., Allen, R., Andrews, M., Bauer, S., Emmons, L., Good, P., Horowitz, L., Nabat, P., Naik, V., Neubauer, D., O Connor, F., Olivie, D., Schultz, M., Sellar, A., Takemura, T., Tilmes, S., Tsigaridis, K., Wu, T., and Zhang, J.: Historical and future changes in air pollutants from CMIP6 models, submitted to Atmospheric Chemistry and Physics, 2020, 2020.

van Marle, M. J. E., Kloster, S., Magi, B. I., Marlon, J. R., Daniau, A.-L., Field, R. D., Arneth, A., Forrest, M., Hantson, S., Kehrwald, N. M., Knorr, W., Lasslop, G., Li, F., Mangeon, S., Yue, C., Kaiser, J. W., and van der Werf, G. R.: Historic global biomass burning emissions for CMIP6 (BB4CMIP) based on merging satellite observations with proxies and fire models (1750–2015), Geoscientific Model Development, 10, 3329–3357, https://doi.org/10.5194/gmd-10-3329-2017, https://www.geosci-model-dev.net/10/3329/2017/, 2017.

Voulgarakis, A., Naik, V., Lamarque, J.-F., Shindell, D. T., Young, P. J., Prather, M. J., Wild, O., Field, R. D., Bergmann, D., Cameron-Smith, P. J., Cionni, I., Collins, W. J., Dalsøren, S. B., Doherty, R. M., Eyring, V., Faluvegi, G., Folberth, G. A., Horowitz, L. W., Josse, B., MacKenzie, I. A., Nagashima, T., Plummer, D. A., Righi, M., Rumbold, S. T., Stevenson, D. S., Strode, S. A., Sudo, K., Szopa, S., and Zeng, G.: Analysis of present day and future OH and methane lifetime in the ACCMIP simulations, Atmos Chem Phys, 13, 2563–2587, https://doi.org/10.5194/acp-13-2563-2013, 2013.

Walters, D., Baran, A. J., Boutle, I., Brooks, M., Earnshaw, P., Edwards, J., Furtado, K., Hill, P., Lock, A., Manners, J., Morcrette, C., Mulcahy, J., Sanchez, C., Smith, C., Stratton, R., Tennant, W., Tomassini, L., Weverberg, K. V., Vosper, S., Willett, M., Browse, J., Bushell, A., Carslaw, K., Dalvi, M., Essery, R., Gedney, N., Hardiman, S., Johnson, B., Johnson, C., Jones, A., Jones, C., Mann, G., Milton, S., Rumbold, H., Sellar, A., Ujiie, M., Whitall, M., Williams, K., and Zerroukat, M.: The Met Office Unified Model Global Atmosphere 7.0/7.1 and JULES Global Land 7.0 configurations, Geoscientific Model Development, 12, 1909–1963, https://doi.org/https://doi.org/10.5194/gmd-12-1909-2019, https://www.geosci-model-dev.net/12/1909/2019/, 2019.

Wild, O. and Palmer, P. I.: How sensitive is tropospheric oxidation to anthropogenic emissions?, Geophysical Research Letters, 35, https://doi.org/10.1029/2008GL035718, https://agupubs.onlinelibrary.wiley.com/doi/abs/10.1029/2008GL035718, 2008.

Williams, K. D., Copsey, D., Blockley, E. W., Bodas-Salcedo, A., Calvert, D., Comer, R., Davis, P., Graham, T., Hewitt, H. T., Hill, R., Hyder, P., Ineson, S., Johns, T. C., Keen, A. B., Lee, R. W., Megann, A., Milton, S. F., Rae, J. G. L., Roberts, M. J., Scaife, A. A., Schiemann, R., Storkey, D., Thorpe, L., Watterson, I. G., Walters, D. N., West, A., Wood, R. A., Woollings, T., and Xavier, P. K.: The Met Office Global Coupled Model 3.0 and 3.1 (GC3.0 and GC3.1) Configurations, Journal of Advances in Modeling Earth Systems, 10, 357–380, https://doi.org/10.1002/2017MS001115, https://agupubs.onlinelibrary.wiley.com/doi/abs/10.1002/2017MS001115, 2018.

Yeung, L. Y., Murray, L. T., Martinerie, P., Witrant, E., Hu, H., Banerjee, A., Orsi, A., and Chappellaz, J.: Isotopic constraint on the twentieth-century increase in tropospheric ozone, Nature, 570, 224–227, https://doi.org/10.1038/s41586-019-1277-1, https://www.nature.com/articles/s41586-019-1277-1, 2019.

Young, P. J., Archibald, A. T., Bowman, K. W., Lamarque, J.-F., Naik, V., Stevenson, D. S., Tilmes, S., Voulgarakis, A., Wild, O., Bergmann, D., Cameron-Smith, P. J., Cionni, I., Collins, W. J., Dalsøren, S. B., Doherty, R. M., Eyring, V., Faluvegi, G., Horowitz, L. W., Josse, B.,

https://doi.org/10.5194/acp-2019-1216
Preprint. Discussion started: 10 February 2020

Lee, Y. H., MacKenzie, I. A., Nagashima, T., Plummer, D. A., Righi, M., Rumbold, S. T., Skeie, R. B., Shindell, D. T., Strode, S. A., Sudo, K., Szopa, S., and Zeng, G.: Pre-industrial to end 21st century projections of tropospheric ozone from the Atmospheric Chemistry and Climate Model Intercomparison Project (ACCMIP), Atmos Chem Phys, 13, 2063–2090, https://doi.org/10.5194/acp-13-2063-2013, 2013.

Young, P. J., Naik, V., Fiore, A. M., Gaudel, A., Guo, J., Lin, M. Y., Neu, J. L., Parrish, D. D., Rieder, H. E., Schnell, J. L., Tilmes, S., Wild, O., Zhang, L., Ziemke, J. R., Brandt, J., Delcloo, A., Doherty, R. M., Geels, C., Hegglin, M. I., Hu, L., Im, U., Kumar, R., Luhar, A., Murray, L., Plummer, D., Rodriguez, J., Saiz-Lopez, A., Schultz, M. G., Woodhouse, M. T., and Zeng, G.: Tropospheric Ozone Assessment Report: Assessment of global-scale model performance for global and regional ozone distributions, variability, and trends, Elem Sci Anth, 6, 10, https://doi.org/10.1525/elementa.265, http://www.elementascience.org/articles/10.1525/elementa.265/, 2018.

Zanis, P., Hadjinicolaou, P., Pozzer, A., Tyrlis, E., Dafka, S., Mihalopoulos, N., and Lelieveld, J.: Summertime free-tropospheric ozone pool over the eastern Mediterranean/Middle East, Atmospheric Chemistry and Physics, 14, 115–132, https://doi.org/https://doi.org/10.5194/acp-14-115-2014, https://www.atmos-chem-phys.net/14/115/2014/, 2014.

Zhang, Y., Cooper, O. R., Gaudel, A., Thompson, A. M., Nédélec, P., Ogino, S.-Y., and West, J. J.: Tropospheric ozone change from 1980 to 2010 dominated by equatorward redistribution of emissions, Nature Geoscience, 9, 875–879, https://doi.org/10.1038/ngeo2827, https://www.nature.com/articles/ngeo2827, 2016.

Zhao, M., Golaz, J. C., Held, I. M., Guo, H., Balaji, V., Benson, R., Chen, J. H., Chen, X., Donner, L. J., Dunne, J. P., Dunne, K., Durachta, J., Fan, S. M., Freidenreich, S. M., Garner, S. T., Ginoux, P., Harris, L. M., Horowitz, L. W., Krasting, J. P., Langenhorst, A. R., Liang, Z., Lin, P., Lin, S. J., Malyshev, S. L., Mason, E., Milly, P. C. D., Ming, Y., Naik, V., Paulot, F., Paynter, D., Phillipps, P., Radhakrishnan, A., Ramaswamy, V., Robinson, T., Schwarzkopf, D., Seman, C. J., Shevliakova, E., Shen, Z., Shin, H., Silvers, L. G., Wilson, J. R., Winton, M., Wittenberg, A. T., Wyman, B., and Xiang, B.: The GFDL Global Atmosphere and Land Model AM4.0/LM4.0: 1. Simulation Characteristics With Prescribed SSTs, J Adv Model Earth Syst, 10, 691–734, https://doi.org/10.1002/2017MS001208, 2018.

Ziemke, J. R., Chandra, S., Duncan, B. N., Froidevaux, L., Bhartia, P. K., Levelt, P. F., and Waters, J. W.: Tropospheric ozone determined from Aura OMI and MLS: Evaluation of measurements and comparison with the Global Modeling Initiative's Chemical Transport Model, J Geophys Res, 111, D19 303, https://doi.org/10.1029/2006JD007089, 2006.

Ziemke, J. R., Chandra, S., Oman, L. D., and Bhartia, P. K.: A new ENSO index derived from satellite measurements of column ozone, Atmospheric Chemistry and Physics, 10, 3711–3721, https://doi.org/https://doi.org/10.5194/acp-10-3711-2010, https://www.atmos-chem-phys.net/10/3711/2010/, 2010.

https://doi.org/10.5194/acp-2019-1216
Preprint. Discussion started: 10 February 2020

Atmospheric Chemistry and Physics Discussions

Historical		UKESM1	CESM2-WACCM	GFDL-ESM4	Mean±1σ
1850-1859	P	3409	2225	2291	2642±665
	L	3155	2155	2225	2511±558
	P-L	254	70	66	130±107
	DD	633	459	471	520±98
	Residual	379	387	404	390±13
1895-1904	P	3492	2331	2418	2747±647
	L	3212	2253	2332	2599±533
	P-L	279	78	86	148±114
	DD	654	481	497	544±96
	Residual	374	403	410	396±19
1925-1934	P	3711	2573	2684	2989±628
	L	3370	2439	2549	2786±509
	P-L	341	134	135	203±119
	DD	694	530	553	592±89
	Residual	353	396	418	389±33
1945-1954	P	3922	2807	2921	3217±614
	L	3522	2628	2734	2961±488
	P-L	400	179	187	255±126
	DD	730	579	611	640±79
	Residual	329	400	424	384±49
1975-1984	P	4677	3699	3822	4066±533
	L	4004	3277	3440	3574±382
	P-L	673	422	382	492±158
	DD	837	725	774	779±56
	Residual	164	303	392	287±115
1995-2004	P	5315	4366	4371	4684±547
	L	4476	3835	3905	4072±352
	P-L	839	530	466	612±200
	DD	867	791	833	830±8
	Residual	28	261	367	219±173

Table 1. Tropospheric ozone budget terms for the three models averaged over each 10-year historical period. P for chemical production, L for chemical loss, P−L for net chemical production, DD for dry deposition, and Residual is the term balance by Residual=L-P+DD.

https://doi.org/10.5194/acp-2019-1216
Preprint. Discussion started: 10 February 2020

Atmospheric Chemistry and Physics Discussions

SSP370		UKESM1	CESM2-WACCM	GFDL-ESM4	Mean±1σ
2025-2034	P	5867	4996	4805	5223±566
	L	4977	4399	4330	4569±355
	P-L	890	597	475	654±213
	DD	894	863	879	879±15
	Residual	4	266	404	225±203
2045-2054	P	6114	5311	4974	5466±586
	L	5273	4756	4535	4855±379
	P-L	841	555	439	612±207
	DD	899	895	898	897±2
	Residual	58	340	459	286±206
2090-2099	P	6763	5909	5324	5999±724
	L	6089	5527	4981	5532±554
	P-L	675	382	343	467±181
	DD	887	909	898	896±8
	Residual	212	522	555	430±189

Table 2. Same as Table 1 but for ssp370

https://doi.org/10.5194/acp-2019-1216
Preprint. Discussion started: 10 February 2020

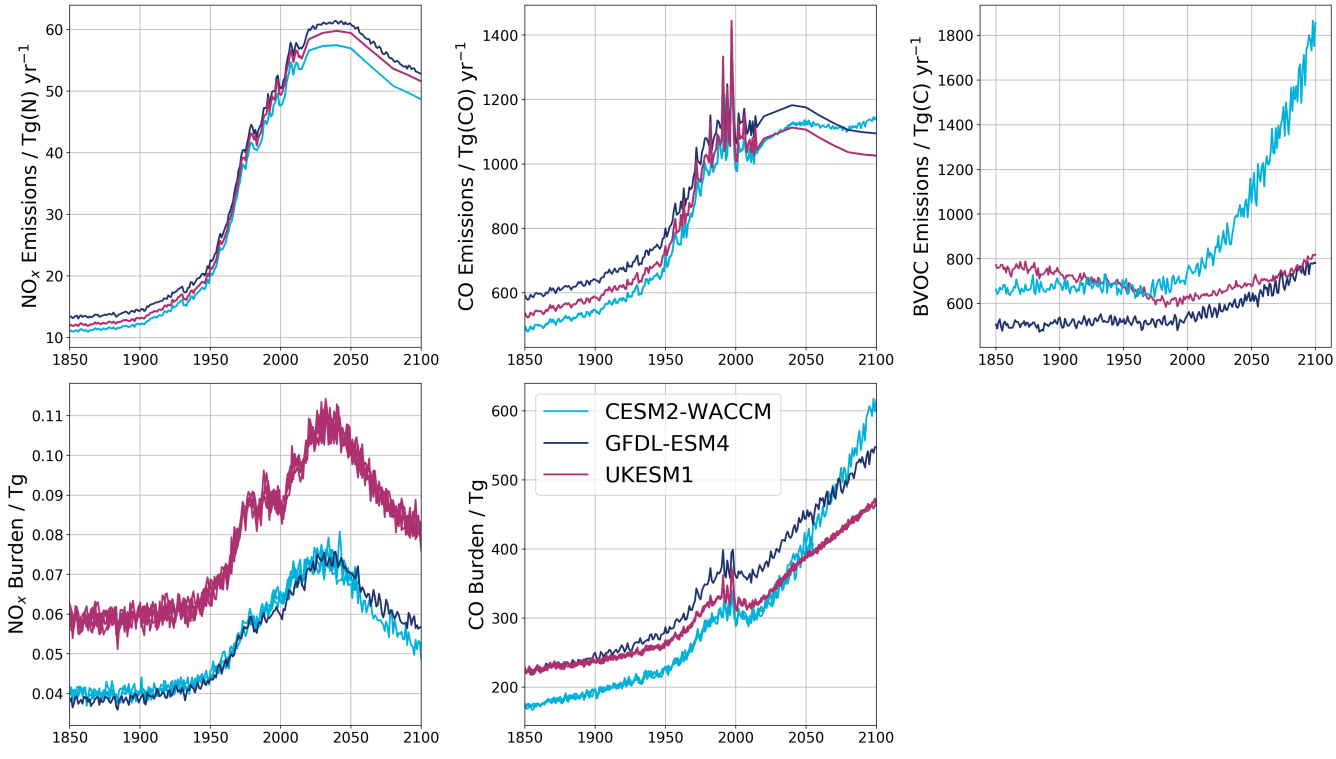

Figure 1. Diagnosed emissions and burden of tropospheric ozone precursors. Maroon line: UKESM1; Light blue line: CESM2-WACCM; Dark blue line: GFDL-ESM4.

https://doi.org/10.5194/acp-2019-1216
Preprint. Discussion started: 10 February 2020

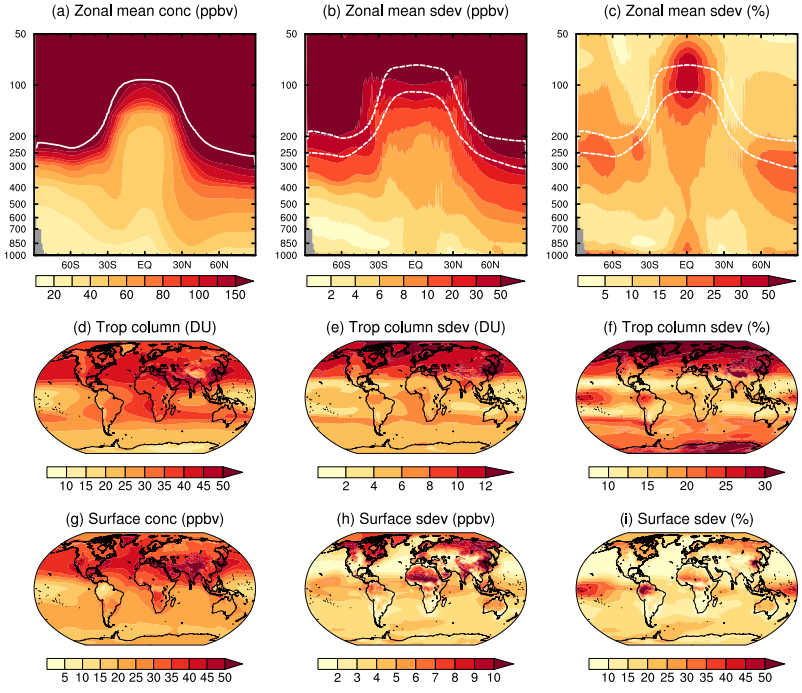

Figure 2. CMIP6 ensemble mean, annual mean ozone climatologies, and their inter-model variability in the present day (2005-2014 .C.E.) of the historical simulation. The top row shows zonal mean ozone, the middle row shows the tropospheric ozone column, and the bottom row shows surface ozone. For each row, the left hand panel shows the absolute values of the ozone variable: ppbv for the zonal mean and surface concentrations, and Dobson units (DU) for the tropospheric column. The middle column shows the absolute inter-model standard deviations in the same units. The right column shows the standard deviation as a percentage of the ensemble mean value. The top row also shows the multi-model zonal mean tropopause pressure (left panel), and the mean $\pm$ one standard deviation of the multi-model variability (middle and right panels). Note that each panel has a different scale. This is an updated version of Fig. 3 of Young et al. (2013).

https://doi.org/10.5194/acp-2019-1216
Preprint. Discussion started: 10 February 2020

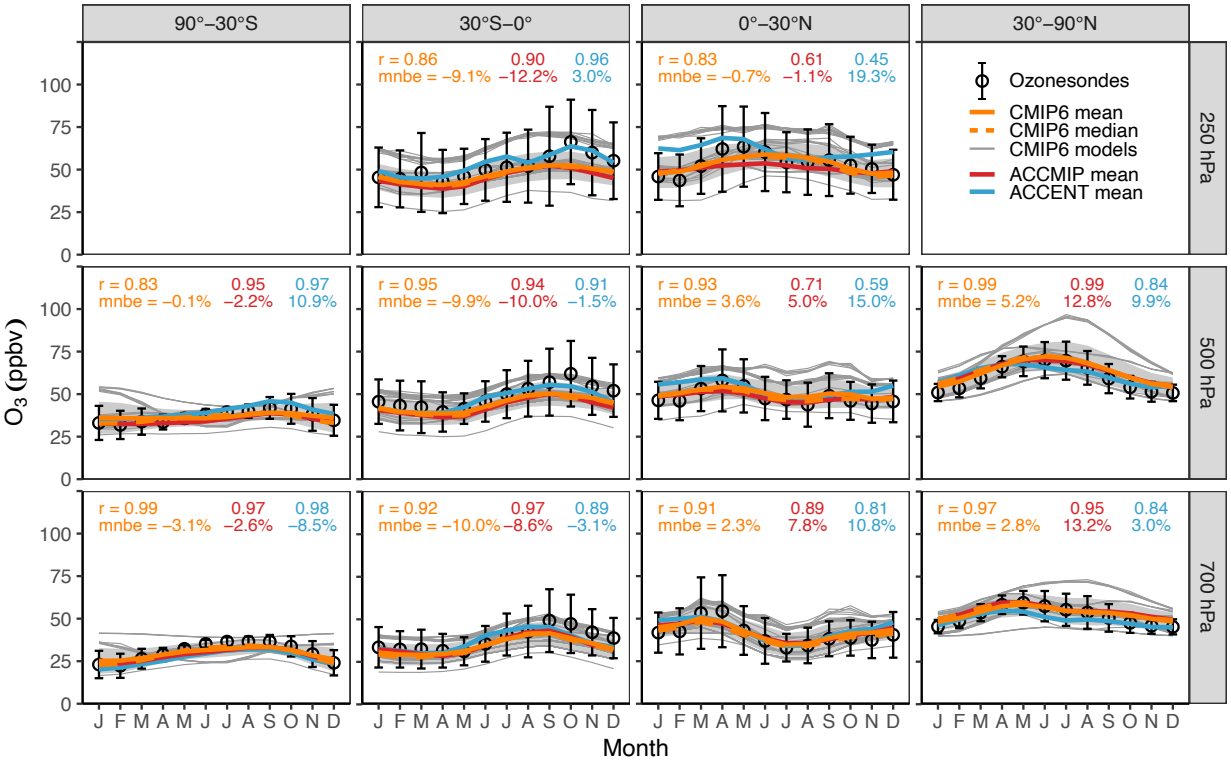

Figure 3. Comparison of the annual cycle of ozone, between ozonesonde observations (black circles) and the CMIP6 ensemble mean (solid orange line), CMIP6 ensemble median (dashed orange line), the ACCMIP ensemble mean (red line; Young et al., 2013) and the ACCENT ensemble mean (blue line; Stevenson et al., 2006). CMIP6 model data is from years 2005 to 2014 of the historical experiment. Model and observational data were grouped into four latitude bands (90°S to 30°S, 30°S to 0°, 0° to 30°N and 30°N to 90°N) and sampled at three altitudes (700 hPa, 500 hPa and 250 hPa), with the models sampled at locations and months of the ozonesonde measurements before averaging together. The individual CMIP6 models and ensemble members are represented by the thin grey lines, with the grey shaded area indicating $\pm$ 1 standard deviation about the CMIP6 ensemble mean. Error bars on the observations indicate the average interannual standard deviation for each group of stations. The correlation (r) and mean normalised bias error (mnbe) for the CMIP6 (orange), ACCMIP (red) and ACCENT (blue) ensemble means versus the observations are also indicated in each panel. This figure is an update of Fig. 4 of Young et al. (2013).

https://doi.org/10.5194/acp-2019-1216
Preprint. Discussion started: 10 February 2020

Atmospheric Chemistry and Physics Discussions

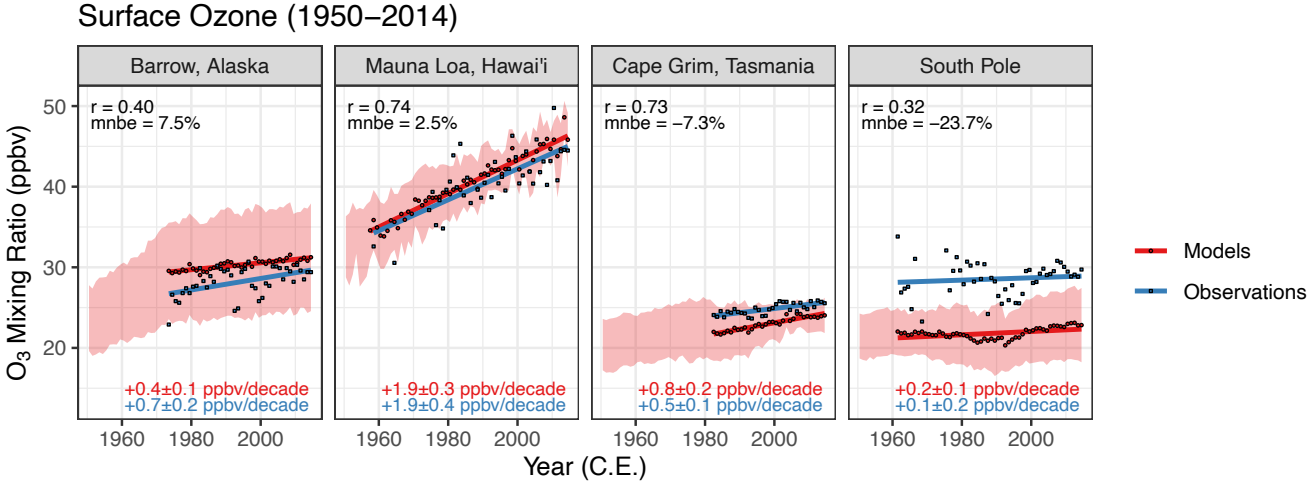

Figure 4. Comparison of annual mean surface observations with the multi-model mean at 4 stations: Barrow, Alaska, USA (71.3°N, 156.6°W, 11 m.a.s.l.), Mauna Loa, Hawai'i, USA (19.5°N, 155.6°W, 3397 m.a.s.l.), Cape Grim, Tasmania, Australia (40.7°S, 144.7°E, 94 m.a.s.l.), and the South Pole (90.0°S, 59.0°E, 2840 m.a.s.l.). The models are sampled from the surface level, except for Mauna Loa, which is sampled at 680 hPa. The pink shading represents the multi-model mean and ± one standard deviation at each location. The red circles indicate the multi-model mean sampled at the month of the observations. The blue squares represent the observations. The solid lines show an ordinary least-squares regression for the multi-model mean and the observations, with the respective slope printed in the lower right of the panel. The temporal correlation (r) and mean normalized bias error (mnbe) are shown in black for each panel.

https://doi.org/10.5194/acp-2019-1216
Preprint. Discussion started: 10 February 2020

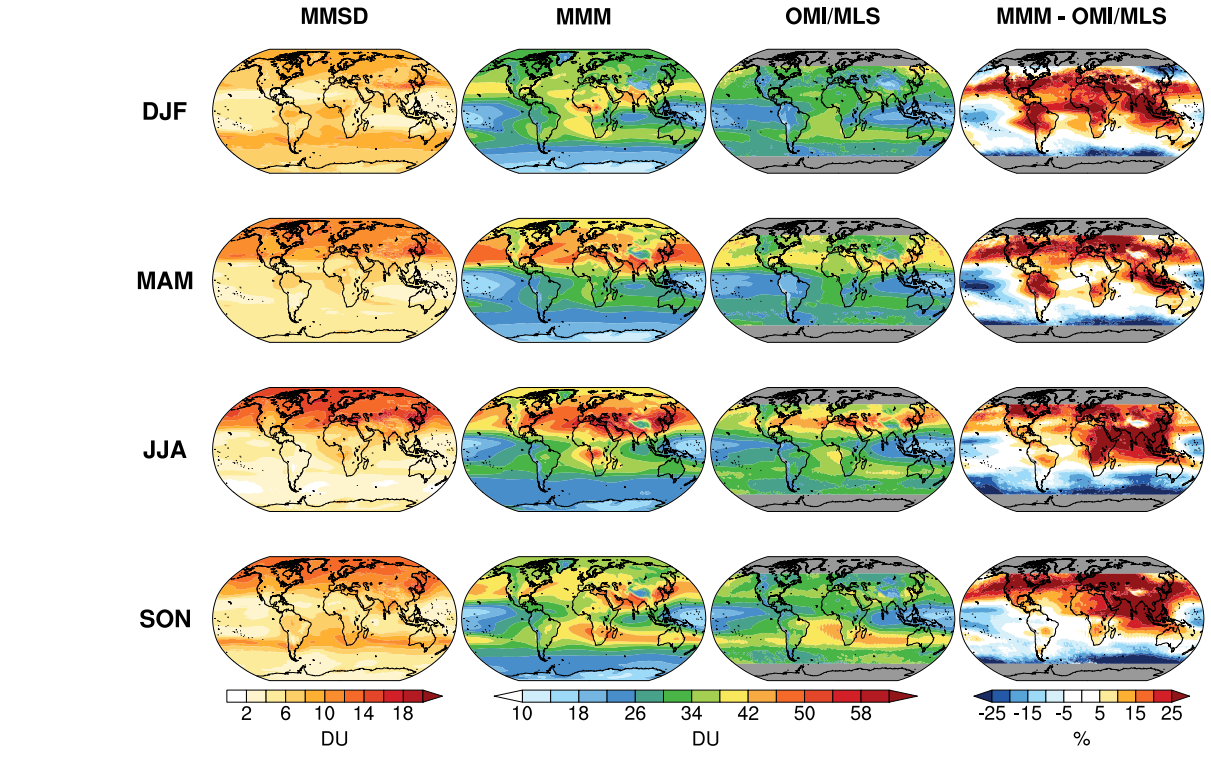

Figure 5. Comparison of the seasonal cycle of tropospheric column of ozone (TCO) abundances with satellite climatology for the period 2005 to 2014. Each row shows a separate meteorological season, from top to bottom: December to February (DJF), March to May (MAM), June to August (JJA), and September to November (SON). The left column shows the inter-model standard deviation of seasonal mean TCO in the CMIP6 ensemble in Dobson Units (DU). The second from the left column shows the multi-model seasonal mean TCO in DU. The second from the right column shows the seasonal mean TCO in the OMI/MLS product (Ziemke et al., 2006). The right column shows the relative bias in the multi-model seasonal mean relative to the OMI/MLS product in percent (%).

https://doi.org/10.5194/acp-2019-1216
Preprint. Discussion started: 10 February 2020

Atmospheric Chemistry and Physics Discussions

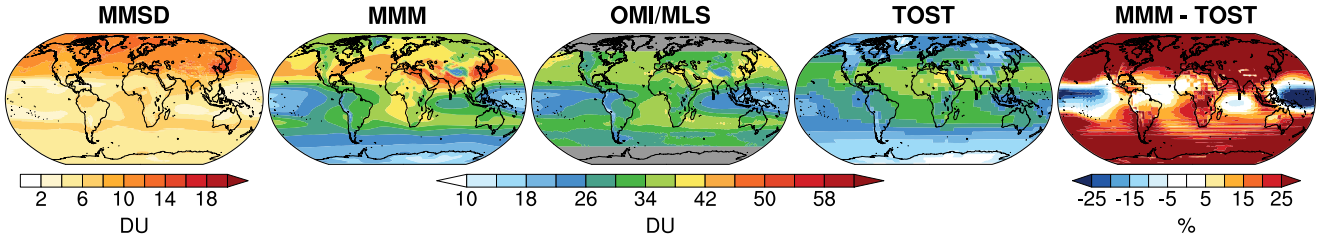

Figure 6. Comparison of the annual tropospheric column of ozone (TCO) abundance with satellite (OMI/MLS) and ozonesonde-derived (TOST) climatologies for the period 2005 to 2014. The left column shows the inter-model standard deviation of annual mean TCO in the CMIP6 ensemble in Dobson Units (DU). The second from the left column shows the multi-model annual mean TCO in DU. The middle column shows the annual mean TCO in the OMI/MLS product (Ziemke et al., 2006). The second from the right column shows the annual mean TCO in the TOST product (Liu et al., 2013b, a). The right column shows the relative bias in the multi-model mean relative to the TOST product in percent (%).

https://doi.org/10.5194/acp-2019-1216
Preprint. Discussion started: 10 February 2020

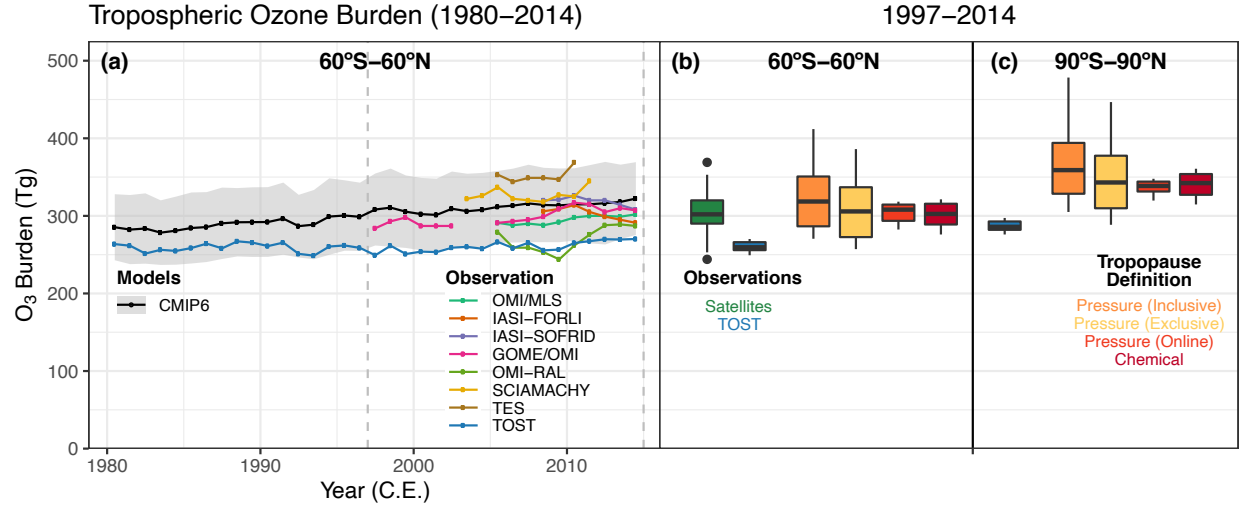

Figure 7. Evaluation of the present-day tropospheric ozone burden. (a) Time series of tropospheric ozone burden integrated from 60°S to 60°N for the period 1980 to 2014 (C.E.). The black line shows the CMIP6 ensemble mean using the pressure tropopause excluding the layer which contains the tropopause. The gray shading shows the mean ± one standard deviation of the ensemble inter-model variability for each year. The coloured lines show the annual mean tropospheric burdens reported by seven satellite products aggregated by Gaudel et al. (2018) and the ozonesonde trajectory product (TOST; Liu et al., 2013b, a). (b) Tropospheric ozone burden distribution for 60°S to 60°N for the period 1997 to 2014 C.E., corresponding to the space between the two vertical dashed lines of panel (a). Box-and-whisker plots show the distribution of the various satellite products (green) and TOST (blue), alongside the CMIP6 ensemble using four different tropopause definitions (see main text for details). (c) The same as panel (b), but showing the burden integrated from 90°S to 90°N in the TOST product and models. All units are in Tg O_3.

https://doi.org/10.5194/acp-2019-1216
Preprint. Discussion started: 10 February 2020

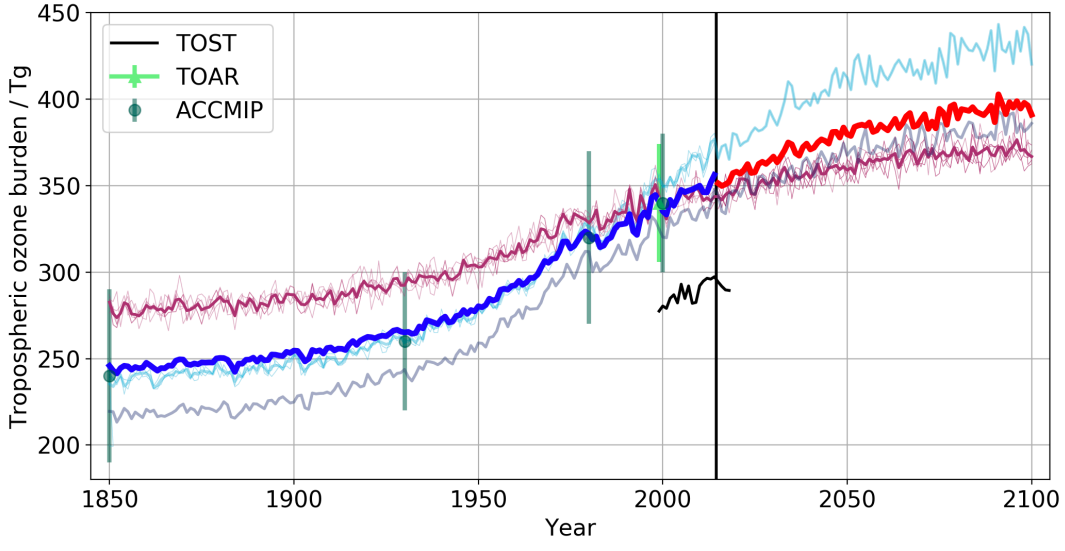

Figure 8. Evolution of tropospheric ozone burden over the period 1850-2100. Models are shown as coloured lines. Maroon line: UKESM1; Light blue line: CESM2-WACCM; Dark blue line: GFDL-ESM4. Blue line: multi-model mean for CMIP Historical experiment. Red line: multi-model mean for ScenarioMIP ssp370 experiment. TOST burden is show as black line, TOAR multi-model mean as light green triangle and ACCMIP multi-model mean for timeslice experiments as dark green circles.

https://doi.org/10.5194/acp-2019-1216
Preprint. Discussion started: 10 February 2020

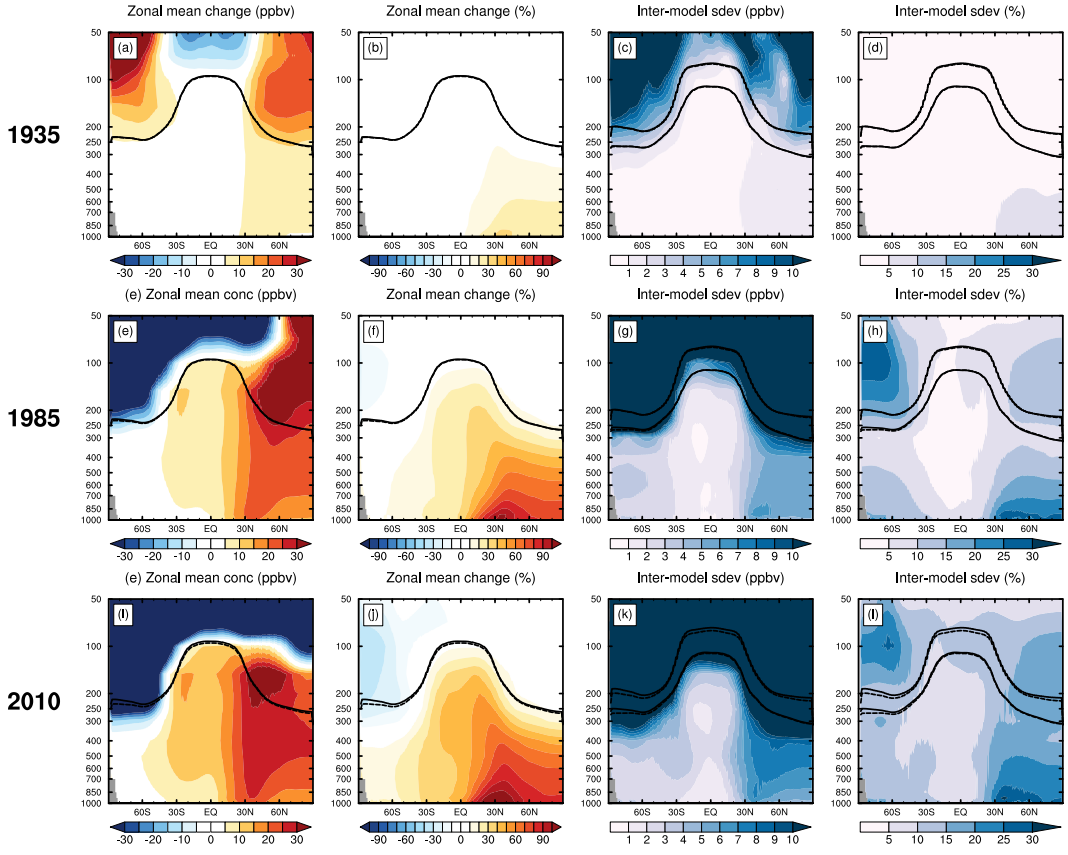

Figure 9. Historic change in zonal decadal mean ozone relative to the preindustrial era. Each row shows the change in decadal zonal (i.e. pressure altitude versus latitude) statistics in the CMIP6 historical simulations relative to those of 1850-1859 C.E. From top to bottom: the change at 1930-1939, at 1980-1989, and at 2005-2014 C.E. The left two columns show the absolute and relative change, respectively, in the ozone mixing ratio in nmol mol^{-1} (ppbv) and in percent (%). Both panels show the multi-model decadal mean tropopause pressure for the relevant decade as a solid black line, and from 1850-1859 C.E. as a dashed black line. The second-from-right column shows the absolute inter-model standard deviation in the simulated change in nmol mol^{-1} (ppbv), and the mean $\pm$ one standard deviation in tropopause pressure height in the respective decade (solid line) versus 1850-1859 C.E. (dashed line). The rightmost column is the same as the second-from-right column, but normalized by the multi-model mean in percent (%).

https://doi.org/10.5194/acp-2019-1216
Preprint. Discussion started: 10 February 2020

Atmospheric Chemistry and Physics Discussions

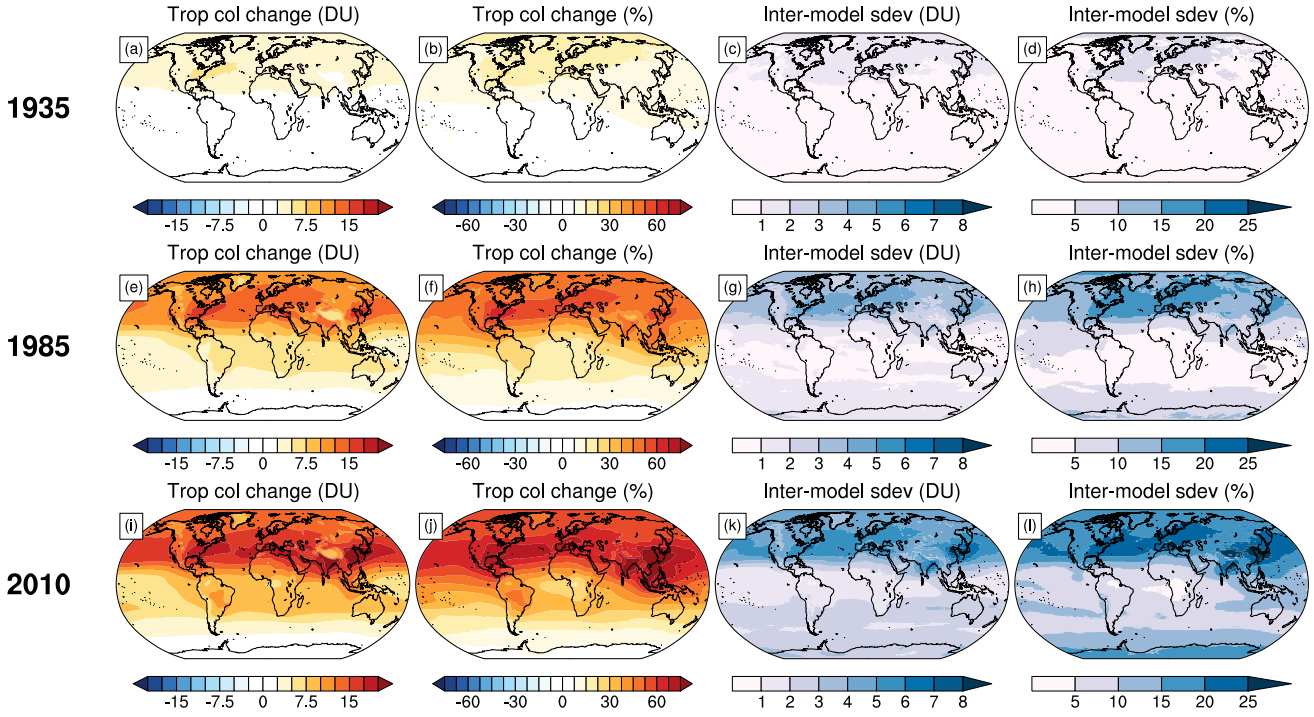

Figure 10. Historic change in tropospheric column ozone (TCO) relative to the preindustrial era. The same as Fig. 9, but for changes in TCO in Dobson Units (DU) or percent (%), as appropriate.

https://doi.org/10.5194/acp-2019-1216
Preprint. Discussion started: 10 February 2020

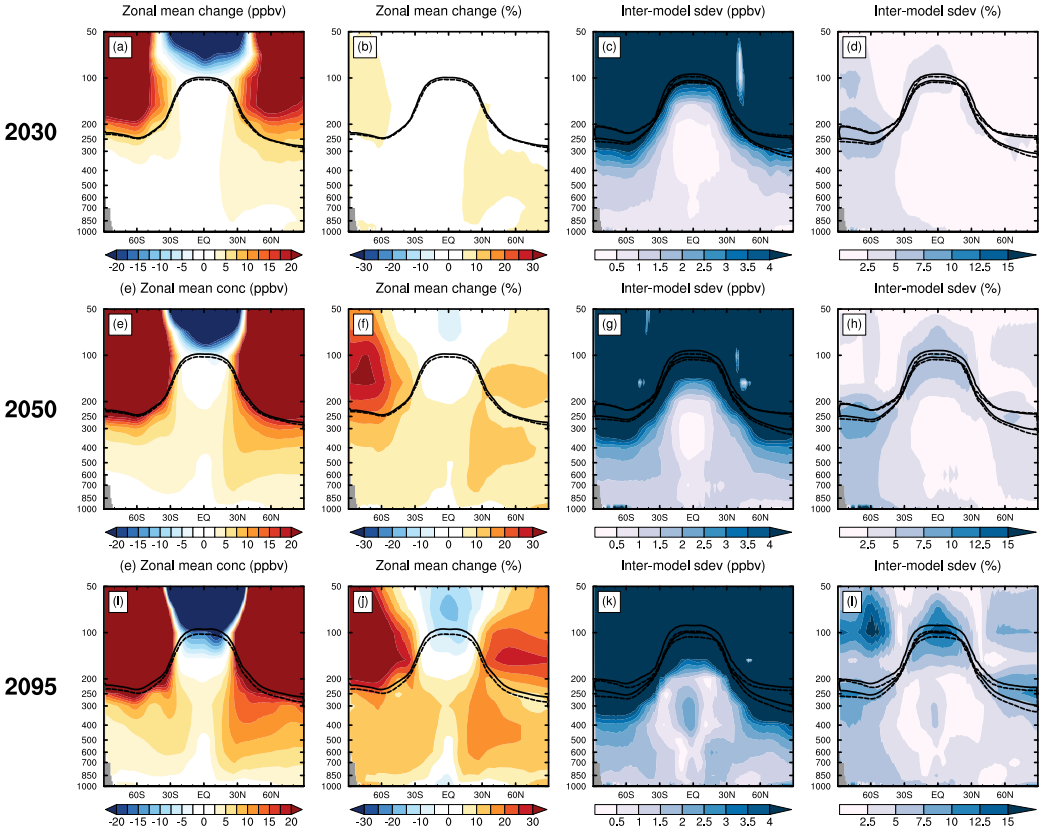

Figure 11. Future change in zonal mean ozone relative to the present day. The same as Fig. 9, but showing future decadal statistics in the ssp370 future scenario relative to 2005-2014 C.E. values. From top to bottom: 2025-2034, 2045-2054, and 2090-2099 C.E.

https://doi.org/10.5194/acp-2019-1216
Preprint. Discussion started: 10 February 2020

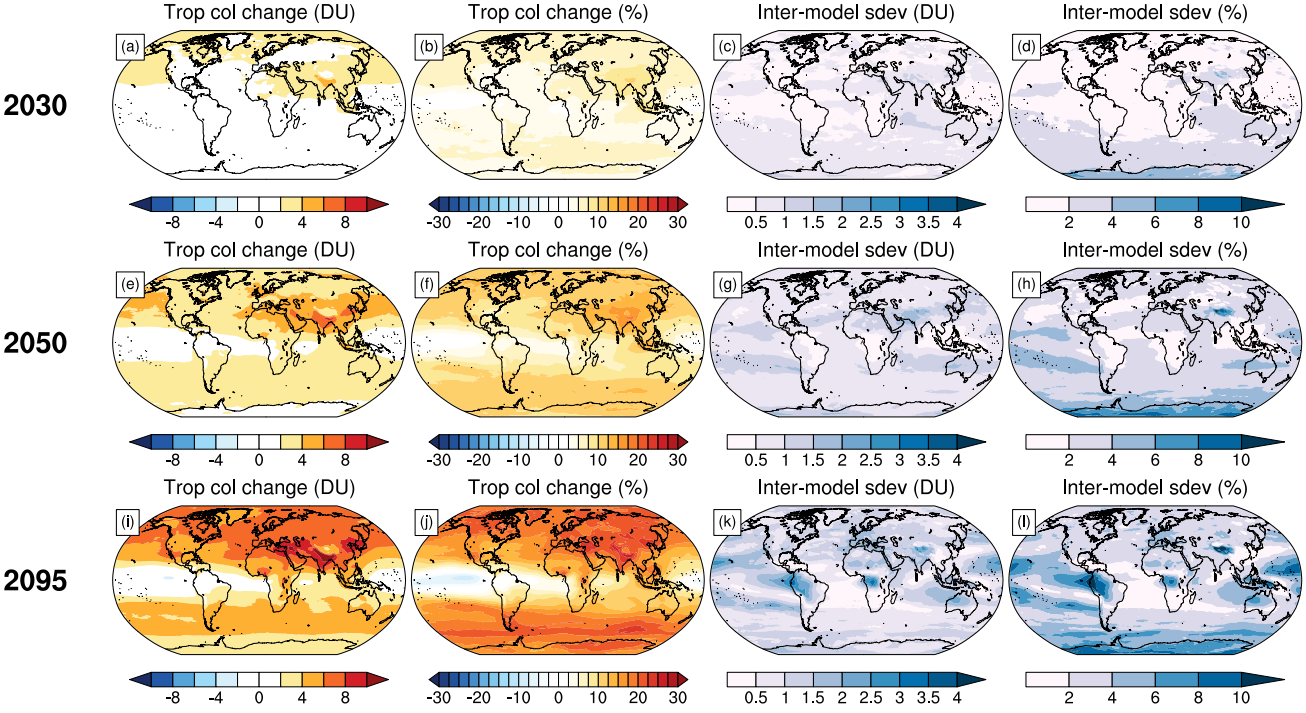

Figure 12. Future change in tropospheric column ozone (TCO) relative to the present day. The same as Fig. 11, but for changes in TCO in Dobson Units (DU) or percent (%), as appropriate.

https://doi.org/10.5194/acp-2019-1216
Preprint. Discussion started: 10 February 2020

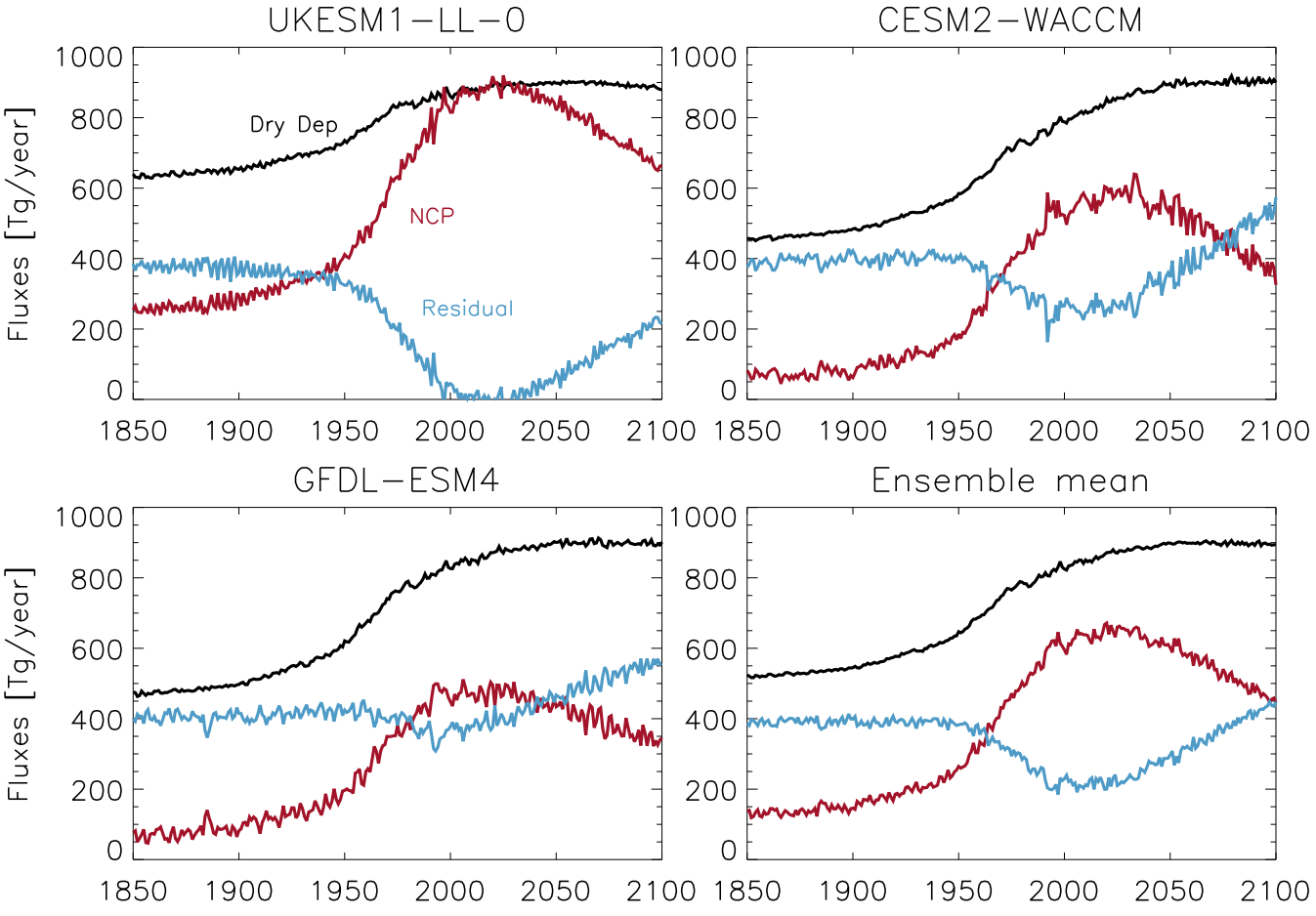

Figure 13. Evolution of net chemical production (red line), dry deposition (black line) and residual ozone budget (blue line) over the period 1850-2100 for three models and the ensemble mean.

https://doi.org/10.5194/acp-2019-1216
Preprint. Discussion started: 10 February 2020

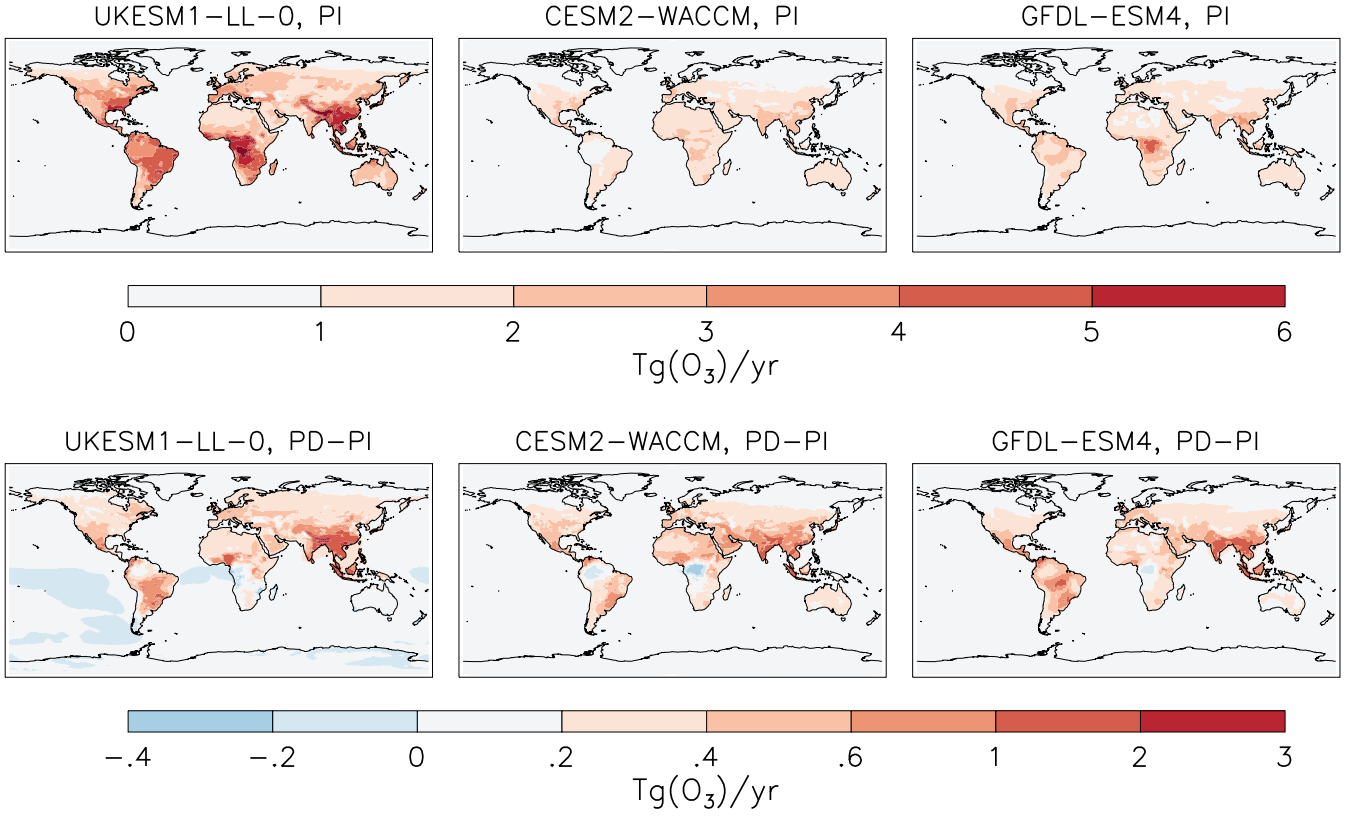

Figure 14. Surface ozone dry deposition for PI period (1850-1859) (top) and the difference between PI and PD (1995-2004) for all three models

https://doi.org/10.5194/acp-2019-1216
Preprint. Discussion started: 10 February 2020

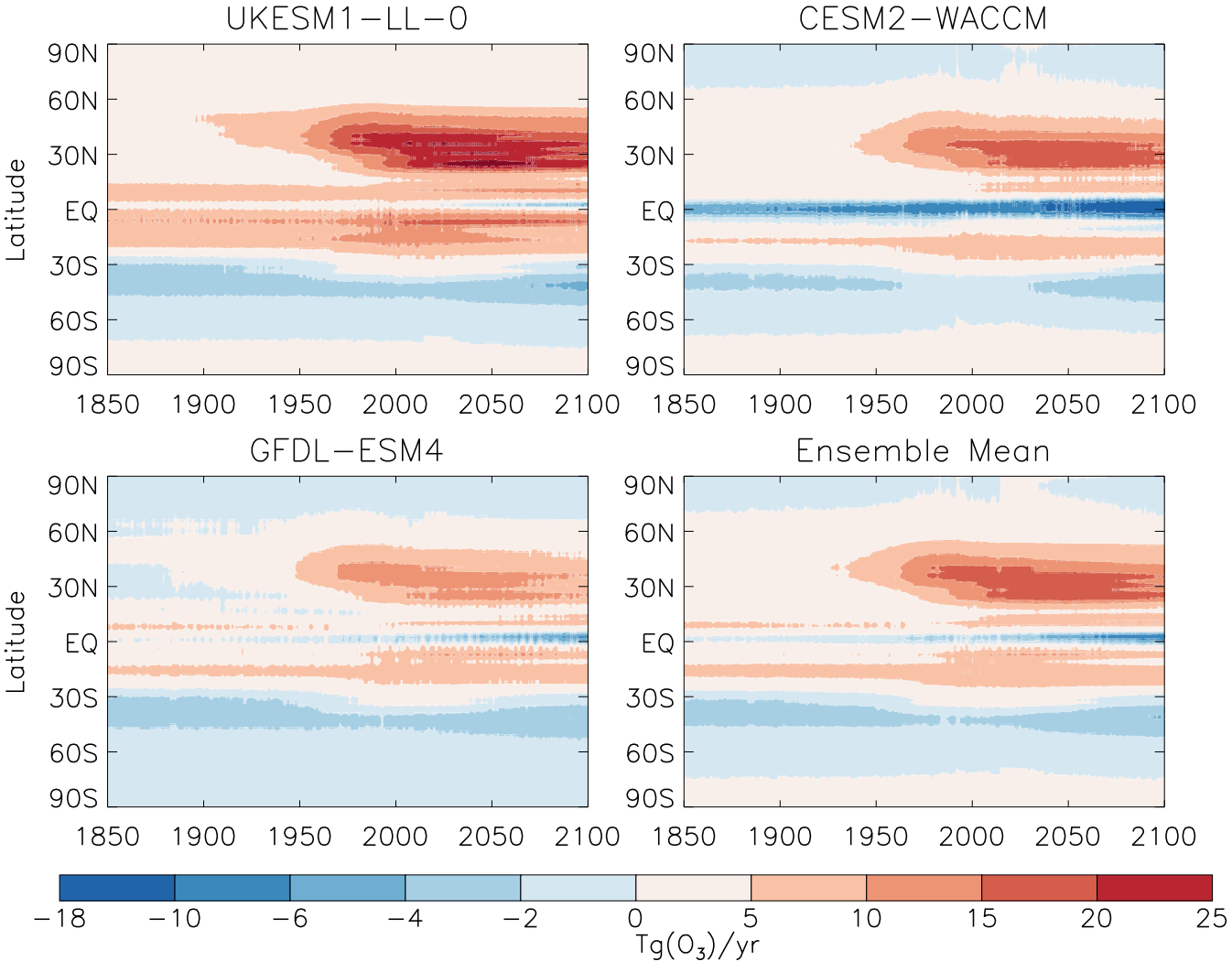

Figure 15. Tropospheric zonal and annual mean net chemical production for UKESM1-LL-0, CESM2-WACCM, and GFDL-ESM4 and the ensemble of these three models. Results are historical (1850-2014) and ssp370 (2015-2100) simulations. Troposphere is masked by the tropopause pressure calculated in each model using the WMO thermal tropopause definition.

https://doi.org/10.5194/acp-2019-1216
Preprint. Discussion started: 10 February 2020

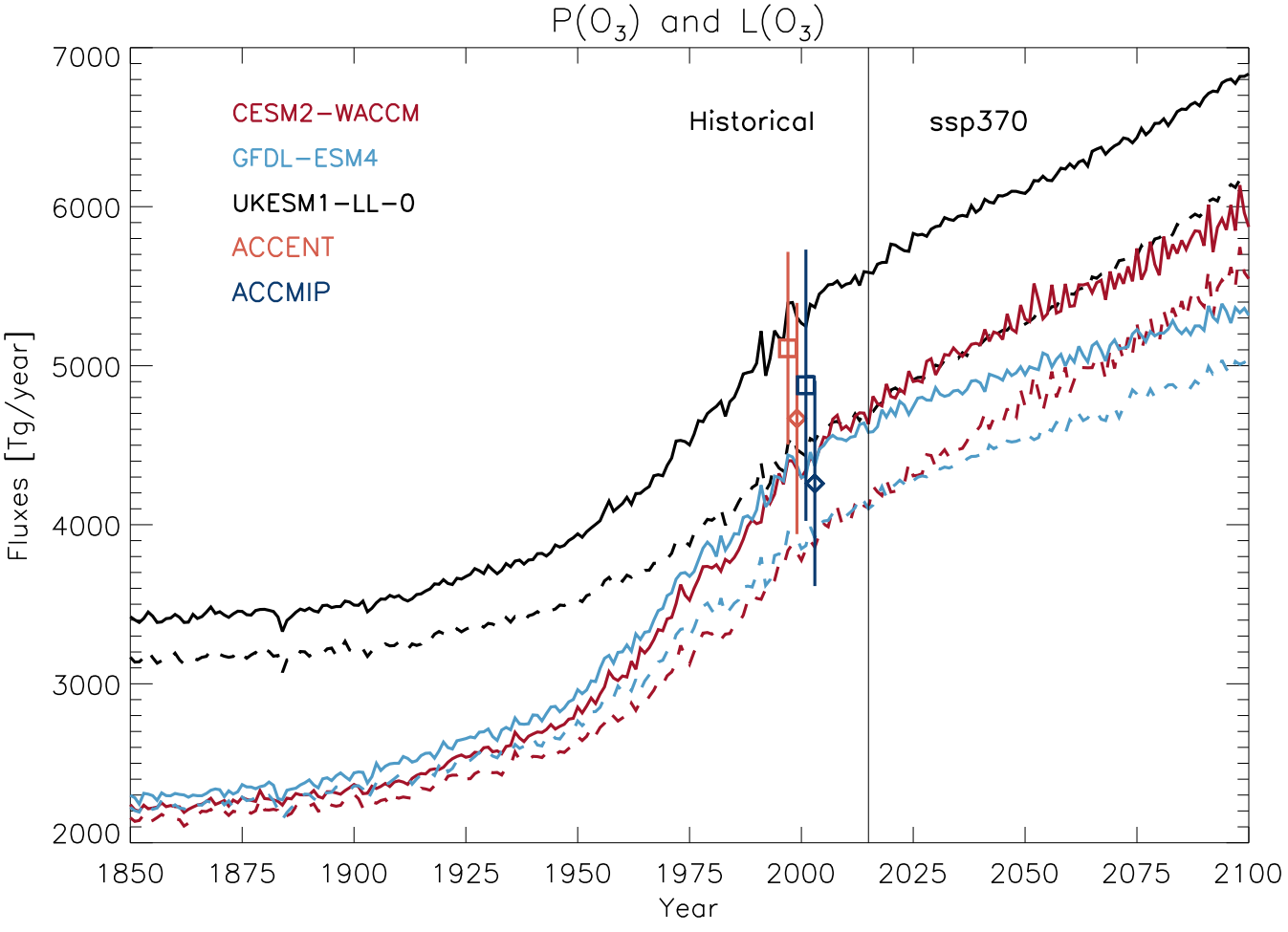

Figure 16. Evolution of ozone production (P, solid line) and loss (L, dashed line) terms from 1850 - 2100 for the three CMIP6 models. ACCENT and ACCMIP production and loss are also display and are for year 2000, but are shifted for displaying purpose, with the symbols denoting mean production (square) and mean loss (diamond).

https://doi.org/10.5194/acp-2019-1216
Preprint. Discussion started: 10 February 2020

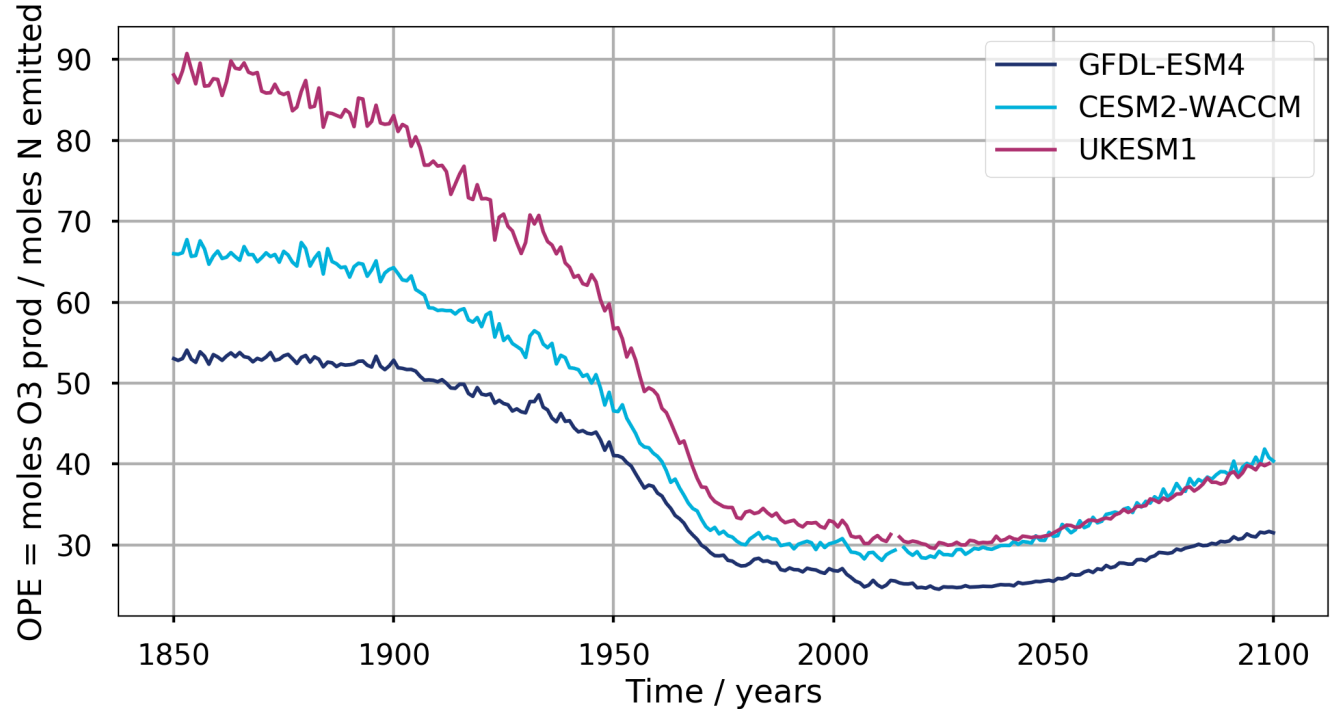

Figure 17. Variation in ozone production efficiency (OPE) for the three models.

https://doi.org/10.5194/acp-2019-1216
Preprint. Discussion started: 10 February 2020

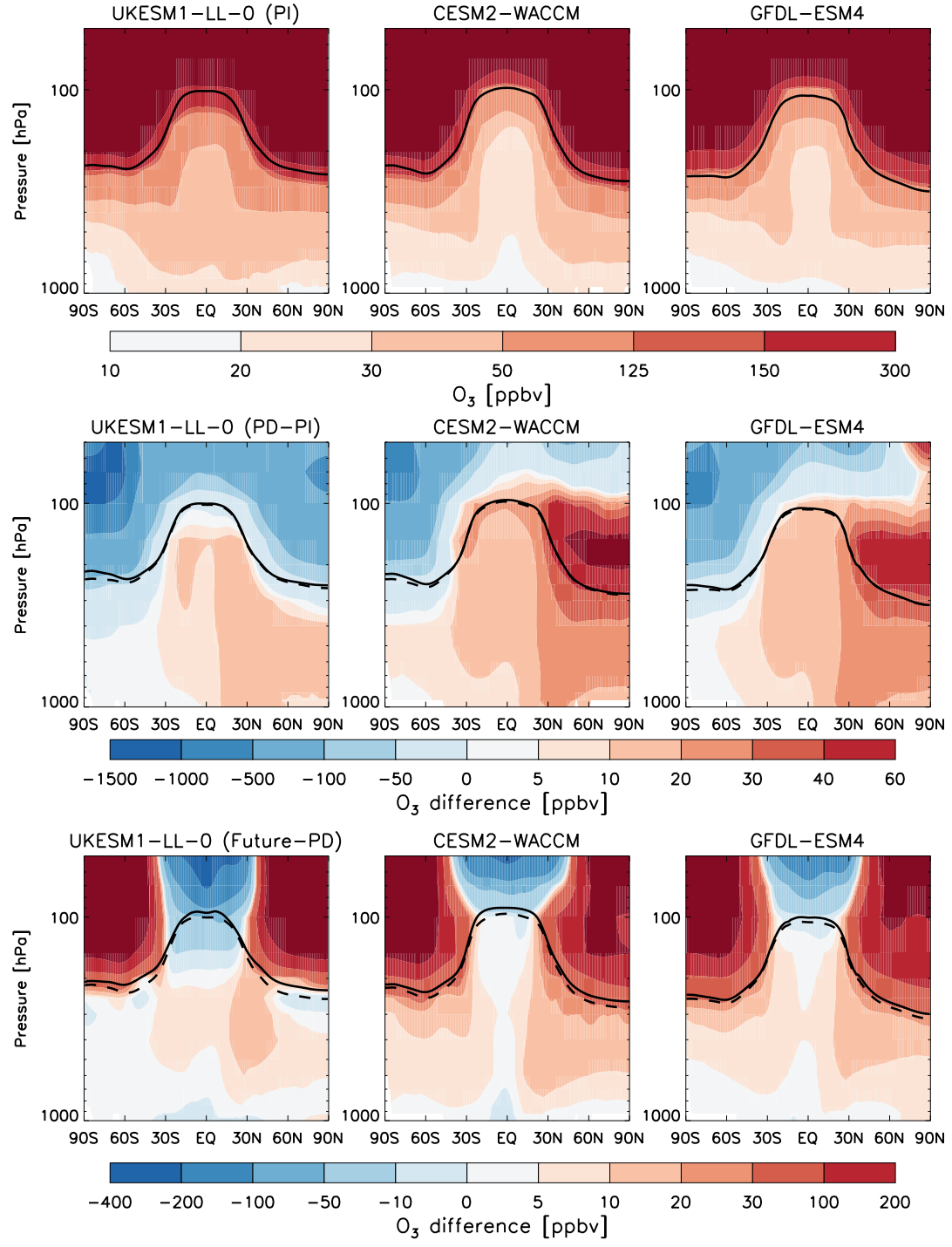

Figure 18. Annual and zonal mean ozone distribution in three models over the PI period (averaged over 1850-1859) (top), the difference between PI and PD (1995-2004) period (bottom), and the difference between PD and future (2090-2099). Thick black lines are the tropopause height of each model based on the WMO definition. Dashed black lines are the tropopause for the PI period in the middle panel, and for the PD period in the bottom panel, respectively.